AGU PUBLICATIONS

JGR

Journal of Geophysical Research: Solid Earth

RESEARCH ARTICLE
10.1002/2014JB011160

Key Points:
- Volatile-rich mantle 5 to 1°N (MAR) derives from the nearby Sierra Leone plume
- H_2O and F from 1°N to 3°S decrease with increasing melting degree
- Four samples dredged at 0.3°S are contaminated by reduced hydrothermal fluids

Supporting Information:
- Readme
- Table S1
- Table S2

Correspondence to:
M. Le Voyer,
mlevoyer@carnegiescience.edu

Citation:
Le Voyer, M., E. Cottrell, K. A. Kelley, M. Brounce, and E. H. Hauri (2015), The effect of primary versus secondary processes on the volatile content of MORB glasses: An example from the equatorial Mid-Atlantic Ridge (5°N–3°S), *J. Geophys. Res. Solid Earth*, *120*, doi:10.1002/2014JB011160.

Received 27 MAR 2014
Accepted 26 NOV 2014
Accepted article online 5 DEC 2014

The effect of primary versus secondary processes on the volatile content of MORB glasses: An example from the equatorial Mid-Atlantic Ridge (5°N–3°S)

Marion Le Voyer[1,2], Elizabeth Cottrell[2], Katherine A. Kelley[3], Maryjo Brounce[3], and Erik H. Hauri[1]

[1]Department of Terrestrial Magnetism, Carnegie Institution of Washington, Washington, District of Colombia, USA, [2]National Museum of Natural History, Smithsonian Institution, Washington, District of Columbia, USA, [3]Graduate School of Oceanography, University of Rhode Island, Narragansett Bay Campus, Narragansett, Rhode Island, USA

Abstract We report microanalysis of volatile and trace element compositions, as well as $Fe^{3+}/\Sigma Fe$ ratios, from 45 basaltic glasses from cruise RC2806 along the equatorial Mid-Atlantic Ridge. The along-strike variations in volatiles result from the complex geodynamical setting of the area, including numerous transform faults, variations in ridge depth, melting degree, and source composition. The strongest gradient is centered on 1.7°N and encompasses an increase of H_2O, Cl, and F contents as well as high F/Zr ratio spatially coincident with radiogenic isotope anomalies. We interpret these variations as source enrichment due to the influence of the nearby high-μ-type Sierra Leone plume. South of the St. Paul fracture zone, H_2O and F contents, as well as H_2O/Ce and F/Zr ratios, decrease progressively. This gradient in volatiles is consistent with progressive dilution of an enriched component in a heterogeneous mantle due to the progressive increase in the degree of melting. These two large-scale gradients are interrupted by small-scale anomalies in volatile contents attributed to (1) low-degree melts preferentially sampling enriched heterogeneities near transform faults and (2) local assimilation of hydrothermal fluids in four samples from dredge 16D. Finally, 20 RC2806 samples described as "popping rocks" during collection do not show any difference in volatile content dissolved in the glass or in vesicularity when compared to the RC2806 "nonpopping" samples. Our observations lead us to question the interpretation of the CO_2 content in the highly vesicular 2πD43 "popping rock" as being representative of the CO_2 content of undegassed mid-ocean ridge basalt.

1. Introduction

Melting of the upper oceanic mantle at mid-ocean ridges generates mid-ocean ridge basalts (MORBs). They provide a direct opportunity to study the compositional variation of the upper mantle. Their major, trace, and isotopic compositions have been extensively studied, and the process of melt generation at spreading centers is now well understood [e.g., *Klein and Langmuir*, 1987]. The main chemical gradients along ridge axes have been described both at the local and at the global scale and are attributed either to changes in the degree of melting or to the presence of heterogeneities in the mantle source. Major chemical anomalies are found near hot spot tracks (e.g., Iceland or Azores) and near transform faults (e.g., Romanche or Chain fracture zones). In the vicinity of a plume, the mantle is hotter, and the magma production is increased, resulting in the presence of a positive topographic anomaly [*Schilling*, 1973; *White and Schilling*, 1978; *Schilling et al*., 1980, 1983]. The plume source can also be enriched in volatiles and radiogenic isotopes, resulting in the presence of a chemical anomaly in the vicinity of the hot spot track. Near transform faults, because of the contact between the ridge axis and cold, older lithosphere, the melt production decreases, and the ridge axis deepens [*Fox and Gallo*, 1984; *Bender et al*., 1984; *Langmuir and Bender*, 1984]. These melts are anomalously enriched in incompatible elements and sometimes in radiogenic isotopes, as small-scale mantle heterogeneities might be preferentially sampled by the low degree of melting near fracture zones. Shallow contamination by seawater or hydrothermally altered material [e.g., *Michael and Cornell*, 1998] also causes local chemical anomalies in the composition of MORBs.

In magmatic systems, volatile elements (C, O, H, F, Cl, and S) play a key role in the physical properties of magmas as well as the eruption dynamics. Most importantly, the amount of H_2O present in the mantle source strongly affects melting and crystallization processes [e.g., *Asimow et al*., 2004]. Defining the volatile composition of

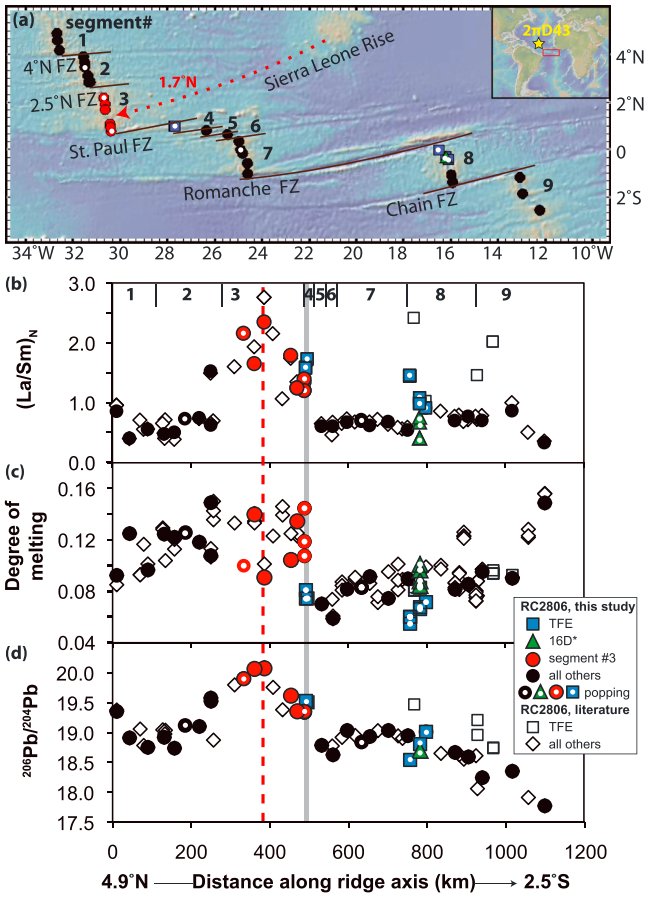

Figure 1. (a) Simplified morphotectonic map of the equatorial MAR showing the location of the RC2806 samples analyzed in this study. The red arrow illustrates the maximum area of influence of the actual Sierra Leone plume. The map was generated with GeoMapApp (http://www.geomapapp.org/) using the Global Multi-Resolution Topography synthesis base map [*Ryan et al.*, 2009], with segment numbers and location of fracture zones from *Schilling et al.* [1994]. TFE: samples affected by transform fault effect (see text). 16D*: 4 samples from dredge 16 that show signs of assimilation of seawater-like material (see text). The location of popping rock sample 2πD43 is shown in yellow on the insert. (b) Variation in $(La/Sm)_N$ (normalized to chondrite [*McDonough and Sun*, 1995]) as a function of cumulative distance along ridge axis (from north to south). Literature data are from *Kelley et al.* [2013]. (c) Variation in degree of melting as a function of cumulative distance along ridge axis. The degree of melting is calculated from $Na_{(8)}$ using Na_2O and MgO contents from *Schilling et al.* [1995], following *Bézos et al.* [2009] and *Langmuir et al.* [1992]. (d) Variation in $^{206}Pb/^{204}Pb$ as a function of cumulative distance along ridge axis. All data are from *Schilling et al.* [1994]. In Figures 1a–1c, the red dotted line indicates the latitude of maximum influence of the Sierra Leone Plume, and the grey line indicates the latitude of the St. Paul fracture zone.

MORBs is critical to understand both volatile cycling and mantle melting at a global scale. However, as shown by previous studies, separating the effects of source heterogeneity, variations in melting regime, degassing, and shallow contamination can be challenging [e.g., *Cushman et al.*, 2004; *le Roux et al.*, 2006]. It is therefore essential to constrain the separate influences of each of these processes on the volatile content of MORBs in order to assess the composition of primary melts and upper mantle.

Here we investigate the extent and scale of upper mantle heterogeneity in volatile elements in the equatorial portion of the Mid-Atlantic Ridge (MAR) between 3°S and 5°N, using the detailed geochemical study of basaltic glasses. This area is particularly complex: previous studies have described strong zonation in the melting regime and the major, trace, and isotopic compositions of the basalts from this area. These zonations are attributed to the combined effect of (1) the nearby Sierra Leone plume, (2) the large cold zone situated just south of the Equator, and (3) the numerous transform faults segmenting the ridge axis [*Bonatti et al.*, 1992; *Schilling et al.*, 1994, 1995; *Hannigan et al.*, 2001; *Tucker et al.*, 2012]. Our approach consists of combining new in situ measurements of volatile contents, trace element contents, and iron speciation together with the previously published major, trace, isotope, and noble gas compositions from the same samples. We aim to differentiate the effects of shallow contamination and secondary magmatic processes (crystallization and degassing) from heterogeneity in the volatile content of the mantle source. Our results bring new insights on the volatile element behavior in hot zones such as the Sierra Leone hot spot, large cold zones such as the one south of the Equator, and local thermal minima near transform faults.

2. Sample Description and Previous Work

We selected 45 fresh glass samples from along the equatorial MAR (5°N to 3°S; Figure 1a). These glasses were sampled from pillow basalts originally dredged from 3440 to 4530 m below sea level (bsl) during the R/V *Conrad*

RC2806 cruise in June–July 1987. Their bulk chemistry, rare earth element abundances, rare gas, and isotopic compositions are described by *Schilling et al.* [1994, 1995], *Hannigan et al.* [2001], *Tucker et al.* [2012], and *Kelley et al.* [2013]. Key points regarding the characteristics of the equatorial MAR are summarized here, but the details from those studies will not be repeated. The equatorial MAR is highly segmented and displaced en echelon left laterally by transform faults. The studied samples are quartz- or olivine-normative tholeiitic basalts dredged on axis along segments #1 to #9 (Figure 1a, using segment numbers from *Schilling et al.* [1994]). North of the St. Paul transform fault, the ridge is affected by the presence of the Sierra Leone plume: glasses around 1.7°N display high $^{206}Pb/^{204}Pb$ (up to 20.1), high $^{87}Sr/^{86}Sr$ (up to 0.7030), low $^{3}He/^{4}He$ (down to 6.77), and other characteristics interpreted as a high-μ(HIMU)-type component [*Schilling et al.*, 1994; *Kelley et al.*, 2013]. This influence is mostly limited to glasses from segment #3 (Figure 1). The ridge just south of the St. Paul transform zone is one of the deepest in the world (up to 4665 m bsl) and produces very low degree melts. Equivalent Na_2O content for an MgO content of 8 wt %, or $Na_{(8)}$ (calculated using the model of *Bézos et al.* [2009] that takes H_2O into account), is up to 3.6 wt %, indicative of a melt fraction down to 0.05 (calculated from $Na_{(8)}$ using *Langmuir et al.* [1992]). Southward from the St. Paul fracture zone, the basalts follow a 600 km long, nearly linear compositional gradient that reflects increases in potential temperature of about 70°C, mean degree of partial melting from 7% to 10%, and inferred crustal thickness from 3 km to 6 km [*Schilling et al.*, 1994, 1995]. This gradient indicates the presence of a large cold zone in the mantle beneath the Equator. Along this gradient, the composition of the basalts transitions from enriched toward more depleted compositions. This variation in degree of melting also has an indirect effect on the radiogenic isotopic composition of the produced melts. In the north, low-degree melts preferentially sample volatile and radiogenic Pb-rich lumps or veins from a heterogeneous mantle. The increase of melting degree toward the south progressively dilutes this enriched signature, producing gradients in isotopic composition that are correlated with the changes in melting degree and major element compositions [*Schilling et al.*, 1994, 1995]. Glasses found at the southernmost extent of this sample suite, around 2–5°S, are some of the most depleted on Earth. Finally, the large-scale variations described above are disturbed by local heterogeneities in the glass compositions, often found next to fracture zones. These samples display one or several of the following characteristics: nepheline-normative compositions, high $Na_{(8)}$, high K_2O/TiO_2 and $(La/Sm)_N$ ratios as well as high Pb and Sr isotope ratios [*Schilling et al.*, 1994, 1995]. They have been interpreted as very local, small degree melts, associated either with the "cold edge effect" or "transform fault effect" (TFE) of the fracture zone, that preferentially sample enriched source heterogeneities [*Schilling et al.*, 1994, 1995]. These samples are identified as "TFE" in Figure 1 (e.g., samples from dredges 7D and 18D, next to the Romanche fracture zone, or 6D and 4D, next to the Chain fracture zone; Table S1 in the supporting information) and plotted with a square symbol on each figure. In this study we will explore how the main characteristics of the equatorial MAR (hot spot influence, melting gradient, and presence of a large cold zone, small-scale effect of transform faults) affect the spatial variations in volatile contents.

Within the 45 samples we selected, 20 of them are "popping rocks" (identified as "PR" on Table S1 in the supporting information and plotted using a white dot in the center of each symbol on all figures); i.e., they were reported to explode once brought back on the deck of the ship (J. G. Schilling, personal communications). This behavior has been described before in several Atlantic cruises, such as Midlante in 1972 (sample CH31-DR11 [*Hekinian et al.*, 1973; *Pineau et al.*, 1976]) or Akademik B. Petrov in 1985 (sample 2πD43 [*Sarda and Graham*, 1990; *Javoy and Pineau*, 1991; *Pineau and Javoy*, 1994]). The 2πD43 popping rock is a famous and unique specimen as it is highly vesicular (17% [*Sarda and Graham*, 1990]), contrary to all other MAR basalts (3% for popping rock CH31-DR11 [*Hekinian et al.*, 1973] and a few percent for other nonpopping MAR basalts [*Chavrit et al.*, 2012]). This sample, together with undegassed melt inclusions from Siqueiros fracture zone [*Saal et al.*, 2002], has been used as reference for the composition of undegassed MORB as well as for the carbon and rare gas contents of the mantle [*Staudacher et al.*, 1989; *Moreira et al.*, 1998; *Cartigny et al.*, 2008; *Tucker et al.*, 2012]. Because of the presence of the 20 popping samples described in the RC2806 suite, this study will allow the description of the dissolved volatile contents from a new suite of popping samples, in comparison with the nonpopping samples from the same area, as well as in comparison with the 2πD43 popping rock.

3. Methods

We selected two fresh, crystal-poor glass chips from each sample. The first chip was doubly polished and used for micro X-ray absorption near-edge structure (μXANES) measurements. The second chip was mounted into

indium, single polished, and used for secondary ion mass spectrometry (SIMS) and laser ablation–inductively coupled plasma–mass spectrometry (LA-ICP-MS) measurements.

3.1. μXANES

$Fe^{3+}/\Sigma Fe$ ratios were determined in 34 samples (Table S1 in the supporting information) using μXANES spectroscopy at beamline X26A of the National Synchrotron Light Source, Brookhaven National Laboratory, following methods described by *Cottrell et al*. [2009]. The $Fe^{3+}/\Sigma Fe$ ratio is quantified by referencing the drift corrected centroid of preedge spectral features (the area-weighted energy of the preedge $1s \rightarrow 3d$ multiplet) to a calibration curve constructed from experimental basaltic glasses with known $Fe^{3+}/\Sigma Fe$ ratios from Mössbauer spectroscopy. The 1σ uncertainty in $Fe^{3+}/\Sigma Fe$ ratio measured by XANES on unknowns for this range of oxidation states is ±0.0045 [*Cottrell et al*., 2009].

3.2. SIMS

Dissolved volatile abundances (H_2O, CO_2, S, Cl, F, and nonvolatile P) were measured in all 45 samples (Table S1 in the supporting information) at the Department of Terrestrial Magnetism, Carnegie Institution, using a Cameca IMS 6f ion microprobe, following an approach modified from *Hauri et al*. [2002]. Before analysis, indium mounts were cleaned using successive baths of distilled water, ethanol, and acetone then dried in a 70°C oven for several days. During analysis, we used a Cs^+, 15 nA primary beam accelerated to 10 kV, with charge compensation provided by an electron flood gun. After 300 s of presputtering, we successively collected signal for 10 s on mass ^{12}C and 5 s on masses $^{17}O^1H$, ^{19}F, ^{30}Si (reference mass), ^{31}P, ^{32}S, and ^{35}Cl. This cycle is repeated 5 times. A set of basaltic standards and blanks [see *Hauri et al*., 2002] were used to perform the calibration and to assess the detection levels (typically lower than 4 ppm for H_2O, 2 ppm for CO_2, 0.2 ppm for S and Cl, and 0.1 ppm for F and P). Each sample was measured 3 times, and combined accuracy and reproducibility were typically better than 10% for CO_2 and 5% for other elements (2 relative standard deviation (RSD)). Standard ALV519-4-1 was mounted together with samples in each indium mount and is used to correct for potential long-term instrumental drift and to assess long-term reproducibility (better than 5%, 2 RSD, for all volatiles, over 2 years).

3.3. LA-ICP-MS

The concentrations of 40 trace elements were measured in all 45 samples (Table S1 in the supporting information) by LA-ICP-MS at the Graduate School of Oceanography, following methods described by *Kelley et al*. [2003] and *Lytle et al*. [2012]. We used a New Wave UP 213 nm Nd:YAG deep penetration laser coupled with a Thermo X-Series II quadrupole ICP-MS. Analyses were run using 70% energy output, 10 Hz repeat rate, and 80 μm spot size, and data were normalized to ^{43}Ca as the internal standard. A set of eight natural glass standards [see *Lytle et al*., 2012] was used to perform the calibration (linear regressions with $R^2 > 0.995$). Each sample was measured 3 times, and combined accuracy and reproducibility are better than 10% (2 RSD) on average for all elements.

4. Results

The compositions of the 45 RC2806 samples are described here, including the 20 popping samples that are plotted using a white dot in the center of each symbol. The trace and volatile element compositions as well as the $Fe^{3+}/\Sigma Fe$ ratios of the popping samples are indistinguishable from the other nonpopping RC2806 samples. Thus, we discuss their compositions together in the following paragraphs.

4.1. Trace Element Compositions of the RC2806 Samples

The trace element contents of the RC2806 samples are plotted together with data from *Kelley et al*. [2013] in Figure 1b and Figure 2. Our LA-ICP-MS results are in very good agreement with the previous results obtained by solution ICP-MS on the bulk glass (less than 10% relative difference on average for rare earth element (REE) and high field strength elements and less than 20% relative difference on average for all other trace elements) and show similar along-axis variations (Figure 1b). As previously described [*Schilling et al*., 1994; *Hannigan et al*., 2001; *Kelley et al*., 2013], the trace element ratios of the RC2806 samples span a large range, from $(La/Sm)_N$ down to 0.3 at the southernmost end of the studied area, up to $(La/Sm)_N = 2.3$ in segment #3 (Figure 1b and Figure 2). Our sample suite contains 28 depleted MORBs, with $(La/Sm)_N < 1$, and 17 enriched MORBs, with $(La/Sm)_N > 1$ (Figure 1b and Figure 2). Of the 17 E-MORB samples, 10 are located close to the

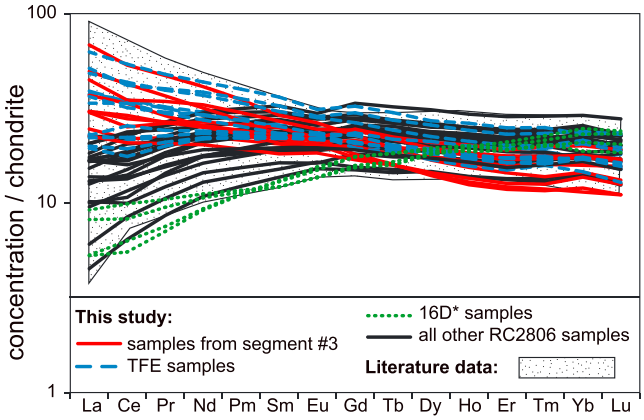

Figure 2. Rare earth element compositions of the RC2806 samples (normalized to chondrite [*McDonough and Sun*, 1995]). Literature data are from *Kelley et al*. [2013].

area of influence of the Sierra Leone hot spot track, around segment #3. The 7 other E-MORBs come from samples affected by TFE. These 7 samples are identified as the TFE subgroup hereafter and will be described separately. Four samples (16D-1 g, 16D-4 g, 16D-5 g, and 16D-6 g) show very contrasting trace element patterns. These 4 samples all come from dredge 16D, near the Romanche fracture zone (green star in Figure 1), and are identified as the 16D* subgroup hereafter. Although they resemble other samples from this area with respect to the depletion in light REE ($(La/Sm)_N$ varying from 0.4 to 0.7), they have higher middle to heavy REE ratios ($(Sm/Yb)_N$ of 0.5–0.7) compared to the other depleted MORBs from this area ($(Sm/Yb)_N$ of 0.9–2.7; Figure 2). The trace element patterns of the 16D* samples also have small positive anomalies in Sr that are not present in other RC2806 samples. These 4 samples will be described separately. Note that the other samples from dredge 16D (i.e., 16D-2 g, 16D-8 g, and 16D-10 g; Table S1 in the supporting information) do not show any of these characteristics and are not included in the 16D* subgroup.

4.2. Iron Speciation of the RC2806 Samples

The average $Fe^{3+}/\Sigma Fe$ ratio of the RC2806 glasses is 0.16 ± 0.01 (2 SD), which corresponds exactly to the global average of worldwide MORBs [*Cottrell and Kelley*, 2011]. The TFE samples do not show anomalous $Fe^{3+}/\Sigma Fe$ ratios compared to the global average or to the other RC2806 samples. However, the $Fe^{3+}/\Sigma Fe$ ratios of the 16D* samples (0.13 ± 0.01 (2 SD)) are significantly lower (3 sigma standard deviations lower) than the global average, which corresponds to a magmatic f_{O2} that is ~0.5 log units more reduced than the global average [*Kress and Carmichael*, 1991].

4.3. Volatile Element Compositions of the RC2806 Samples

4.3.1. Main Group of Samples

In this section we focus on the main group of RC2806 samples, i.e., excluding 16D* and TFE samples, that are described separately in the next two sections. Samples from the main group contain 143 to 264 ppm CO_2, 0.08 to 0.89 wt % H_2O, 82 to 519 ppm F, 8 to 467 ppm Cl, and 1006 to 1331 ppm S (Figures 3, 4, and 5). While the CO_2 and S contents do not show any variation along the ridge axis, the H_2O, F, and Cl contents range significantly, with maxima (sample 40D-9 g) at 1.7°N, similar to $(La/Sm)_N$ or $^{206}Pb/^{204}Pb$ maxima (Figure 1). Note that the southernmost sample (1D-1 g) has the lowest H_2O and F contents of the entire area. Similarly, when plotting the volatile contents of each sample as a function of their MgO contents (Figure 4), we see that most of the samples from segment #3 have higher H_2O, F, and Cl contents at a given MgO, compared to the samples from other segments. For all other segments, the H_2O and F contents are negatively correlated (R^2 of 0.66 and 0.64, respectively), while the Cl contents (except for TFE samples) do not show any clear trend with respect to MgO content. Although the S contents show a negative correlation with MgO ($R^2 = 0.54$; Figure 4), they also show a stronger, negative correlation with FeO contents (Figure 5a).

We calculate the vapor saturation pressure for each sample using the H_2O-CO_2 saturation model from *Dixon and Stolper* [1995]. Vapor saturation pressures (Psat) vary from 326 to 592 bars (Figure 5b). The lowest saturation pressures are found in samples from segment #3. The CO_2 contents of the RC2806 samples do not show any correlations with MgO contents (Figure 4e) or other major or trace element contents. However, they are roughly correlated with their eruption pressure; i.e., the deepest samples tend to have the highest CO_2 contents.

4.3.2. TFE Samples

Samples from the TFE subgroup (i.e., samples located near transform faults with low degree of melting and enriched compositions in trace elements and/or radiogenic isotopes) contain from 181 to 240 ppm CO_2, 0.34

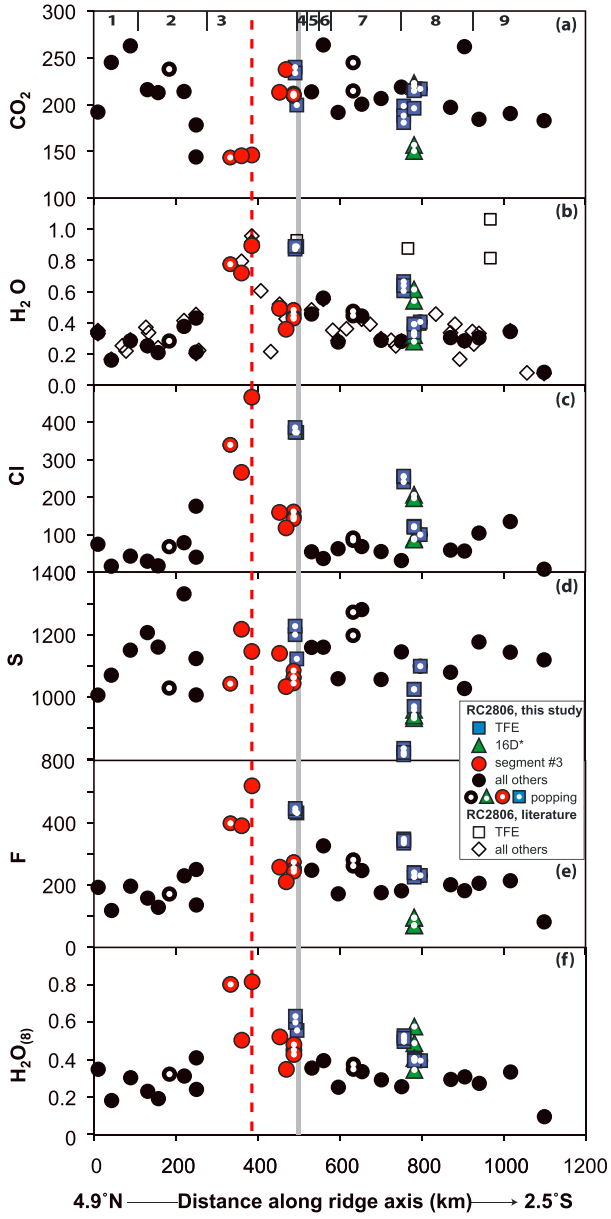

Figure 3. (a) CO_2, (b) H_2O, (c) Cl, (d) S, (e) F, and (f) $H_2O_{(8)}$ contents as a function of distance along the ridge axis. $H_2O_{(8)}$ is calculated using Na_2O and MgO contents from *Schilling et al.* [1995], following the expression of *Taylor and Martinez* [2003]. Literature values for H_2O are from *Schilling* [2014]. The red dotted line indicates the latitude of maximum influence of the Sierra Leone Plume, and the grey line indicates the latitude of the St. Paul fracture zone.

to 0.89 wt % H_2O, 214 to 446 ppm F, 100 to 386 ppm Cl, and 815 to 1228 ppm S (Figures 2–4). Their range in volatile contents is similar to those of other RC2806 samples. However, when plotted as a function of distance along the ridge axis, TFE samples tend to have higher H_2O, F, and Cl contents than their neighbor samples. Moreover, when plotting the volatile contents of each sample as a function of their MgO contents, TFE samples (squares in Figure 4) seem to follow a trend parallel to the one defined by the rest of the RC2806 samples but with higher H_2O, F, and Cl contents at a given MgO content than most of the RC 2806 samples. Samples 18D-1 g, 18D-2 g, and 18D-3 g have lower S contents at a given MgO content than the rest of the TFE samples (Figure 4). They also have much lower FeO contents (7.5–7.7 wt %) compared to all other RC2806 (8.7–11.4 wt %; Figure 5a).

4.3.3. 16D* Samples

Samples from the 16D* subgroup (i.e., the four samples from dredge 16D with contrasting trace element composition and iron speciation) contain 150 to 223 ppm CO_2, 0.28 to 0.61 wt % H_2O, 71 to 96 ppm F, 87 to 207 ppm Cl, and 932 to 959 ppm S (Figures 2–4). Their volatile element contents are within the range of compositions from other RC2806 samples, although they are at the lower end of the F and S ranges (average compositions of 83 ppm F and 943 ppm S, compared to 231 ppm F and 1122 ppm S for other RC2806 samples). When plotting the volatile contents of each sample as a function of the distance along the ridge axis, the 16D* samples tend to have higher H_2O and Cl contents but lower F and S contents compared to nearby samples (Figure 3). Similarly, when plotted as a function of their MgO contents (triangles in Figure 4), we see that the 16D* samples plot away from the main trend, with higher H_2O and Cl contents but lower F and S contents for a given MgO content.

4.3.4. H_2O Content Corrected for Fractional Crystallization ($H_2O_{(8)}$)

In Figure 4, the negative correlation between H_2O contents and MgO contents reflects the effect of fractional crystallization on the H_2O content of the melt. We used the expression from *Taylor and Martinez* [2003] in order to correct for this effect and calculate the H_2O content for each sample for an equivalent MgO content of 8 wt % or $H_2O_{(8)}$. $H_2O_{(8)}$ of the RC2806 samples varies from 0.09 to 0.82 wt %, with an average of 0.36 ± 0.15 (1 SD). The highest $H_2O_{(8)}$ are recorded for samples from segment #3 (Figure 3f). Samples from

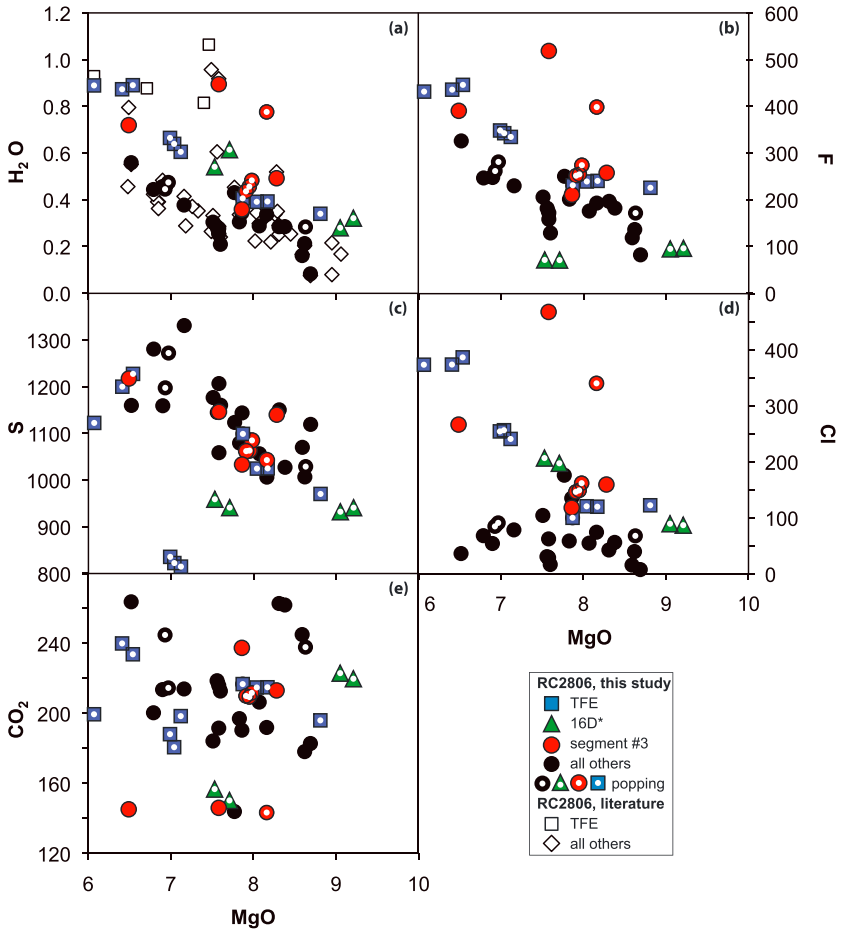

Figure 4. (a) H_2O, (b) F, (c) S, (d) Cl, and (e) CO_2 contents as a function of MgO contents. MgO contents are from *Schilling et al*. [1995]. Literature values for H_2O are from *Schilling* [2014].

16D* and TFE also tend to have higher $H_2O_{(8)}$ content than nearby samples. Finally, samples from segments #5 to #9 display a general decrease in their $H_2O_{(8)}$ from north to south (linear decrease of $R^2 = 0.45$ as a function of distance along the ridge axis), with the lowest $H_2O_{(8)}$ content found in the southernmost sample (1D-1 g; Figure 3f).

5. Discussion

The aim of this discussion is to use our trace and volatile element data set, combined with results from previous studies, to discuss the current model of magma generation along the equatorial MAR. In particular, we want to assess the presence of thermal and/or chemical gradients in the mantle source at small scales, using local anomalous samples (16D* and TFE samples), and at larger scales, using along-ridge gradients. To account for variations in the degree of melting and/or crystallization, we compare each volatile with a trace element with similar compatibility during mantle melting (H_2O with Ce, CO_2 and Cl with Nb, F with Zr, and S with Dy; following *Saal et al*. [2002]; Figures 6 and 7). In Figure 6, a suite of cogenetic samples unaffected by degassing and/or secondary processes should plot on a linear trend going through the origin. While CO_2 and S do not display such correlations relative to Nb and Dy, respectively, the H_2O, Cl, and F contents of most RC2806 samples are positively correlated with Ce, Nb, and Zr contents, respectively, with 16D* samples being outliers compared to the main trend. These correlations go through the origin (R^2 of 0.83, 0.98, and 0.37, respectively) and indicate that we can use the H_2O/Ce, Cl/Nb, and F/Zr ratios as source proxies, although we cannot similarly use CO_2/Nb or S/Dy. The lack of a correlation that goes through the origin between CO_2

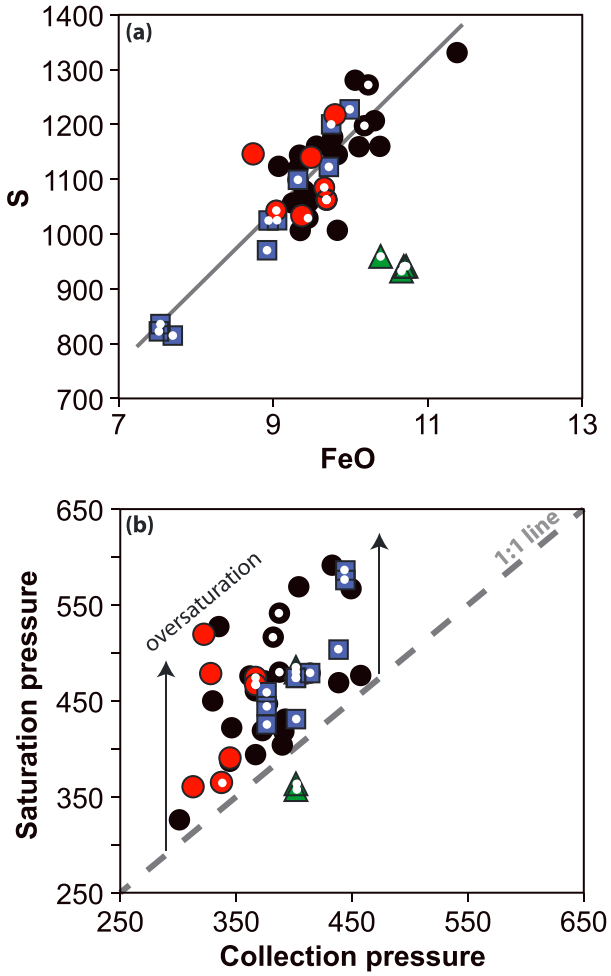

Figure 5. (a) S contents as a function of FeO contents for the RC2806 samples. FeO contents are from *Schilling et al*. [1995]. The straight line corresponds to the linear regression through all samples, except the 16D* samples, and illustrates the covariation of FeO and S under sulfide-saturated conditions. (b) Comparison of the collection pressure in bar (taken as a proxy for eruption pressure) and saturation pressure in bar (calculated using *Dixon and Stolper* [1995]) for all RC2806 samples. Most samples are plotted in the area of sursaturation (i.e., above the 1:1 line). Legend is the same as in Figure 4.

and Nb and S and Dy indicates that S and CO_2 compositional variations in the RC2806 samples cannot be accounted for solely by the effect of variable degree of melting and crystallization for a suite of cogenetic samples. In the first two parts of the discussion, we focus on understanding the processes responsible for the S and CO_2 compositional variations in the RC2806 samples. In the second part, we focus on the 16D* and TFE samples and interpret their contrasting H_2O, F, and Cl compositions as a result of small-scale processes. In the third part of the discussion, we focus on all other RC2806 samples; describe the variations of H_2O/Ce, Cl/Nb, and F/Zr along the ridge axis; and discuss the large-scale processes for melt generation and evolution along the equatorial MAR.

5.1. Case of S: Role of Sulfides

Unlike other volatile elements and incompatible trace elements, the S contents of the RC2806 samples do not show consistent trends together with most physical or geochemical parameters (Figures 4 and 6). The lack of a correlation between sampling depth and sulfur content indicates that S is likely not lost to a vapor phase in the RC2806 samples, similar to other MORB samples [*Jenner et al*., 2010]. We observe a negative correlation between S and MgO and a positive correlation between the S contents and the FeO contents (Figure 5a; excluding samples 16D*). The increase in FeO in the RC2806 samples is correlated with a decrease in MgO and is a typical feature of MORB fractionation. Under the reduced and relatively anhydrous conditions prevailing during MORB fractionation, all S is present as S^{2-} [*Jugo et al*., 2010], and the S content at sulfide saturation is primarily a function of the FeO content [*Li and Naldrett*, 1993; *O'Neill and Mavrogenes*, 2002]. If a magma is sulfide saturated, then as crystallization proceeds and the FeO* content of the magma increases while MgO decreases, the S content will also increase, giving rise to a positive correlation between S and FeO* (Figure 5a) [e.g., *Jenner et al*., 2010] and a negative correlation between S and MgO (Figure 4c). Similarly, the positive correlation between the Cu/S ratio and the MgO contents, and between the Cu and MgO contents of the RC2806 samples (not shown here), results from the effect of sulfide saturation [*Jenner et al*., 2012]. These results suggest that the RC2806 samples are sulfide saturated, similar to most MORB samples [*Mathez*, 1976; *Czamanske and Moore*, 1977; *Wallace and Carmichael*, 1992; *Perfit et al*., 1999]. This is in good agreement with the fact that the three samples with lower FeO contents compared to the rest of the samples (Figure 5a) also have significantly lower S contents. Because the S/Dy ratio is not constant as a function of MgO, and therefore not constant during fractionation, the S/Dy ratio of the melt is not representative of the S/Dy ratio of their mantle source. This implies that the S/Dy ratio cannot be directly used as a tracer of source heterogeneity (Figure 7a). We observed a weak positive

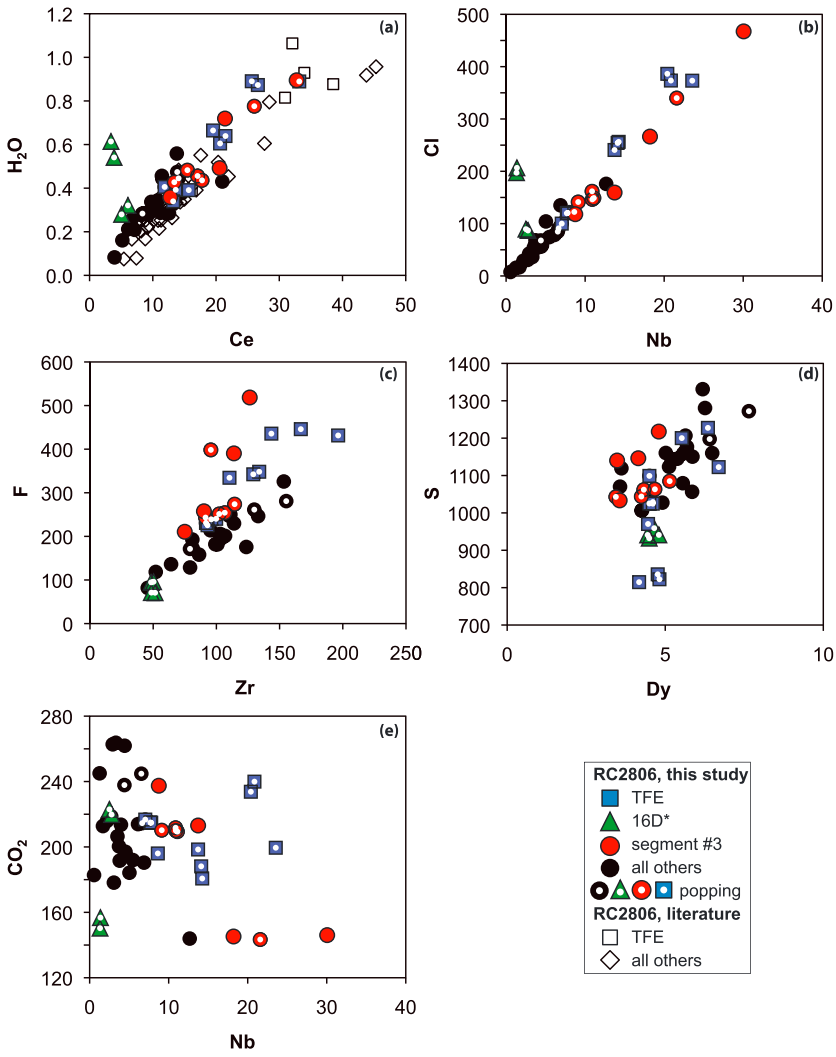

Figure 6. (a) H_2O as a function of Ce, (b) Cl as a function of Nb, (c) F as a function of Zr, (d) S as a function of Dy, and (e) CO_2 as a function of Nb. In Figure 6a, literature values for H_2O are from *Schilling* [2014].

correlation between S and V, and the S/V ratio is constant (4.5 ± 0.9, 2 SD) as a function of MgO. Thus, the S/V ratio seems to remain constant during the overall fractionation path of the RC2806 sample suite and therefore could be used as a proxy for source composition. The S/V ratio does not show any variation as a function of distance along the ridge axis (not shown here), indicating that the S/V ratio of the mantle source beneath the equatorial MAR seems to be constant.

As noted above, the 16D* samples plot as outliers in Figure 5a. In this paragraph, we consider four scenarios to explain their origin. In the first scenario, the 16D* samples could be partially degassed, thus having lost part of their initial S content to a vapor phase, although this scenario is unlikely for samples collected 4 km below sea level. In the second scenario, the 16D* samples could be undersaturated with respect to sulfide, similar to the Siqueiros melt inclusions [*Saal et al.*, 2002]. This could explain their low S contents at a given FeO content, compared to the other RC2806 samples. However, the overall decrease in Cu content as a function of MgO content found in the RC2806 samples, including the 16D* samples (not shown here, $R^2 = 0.3$), is attributed to the fractionation of monosulfide solid solution [*Jenner et al.*, 2010, 2012]. Although this correlation is weak, it indicates that the 16D* samples should be sulfide saturated, similarly to other RC2806 samples. In the third scenario, we consider that the 16D* samples are sulfide saturated but have a lower S content at sulfide saturation compared to other RC2806 samples. S content at sulfide

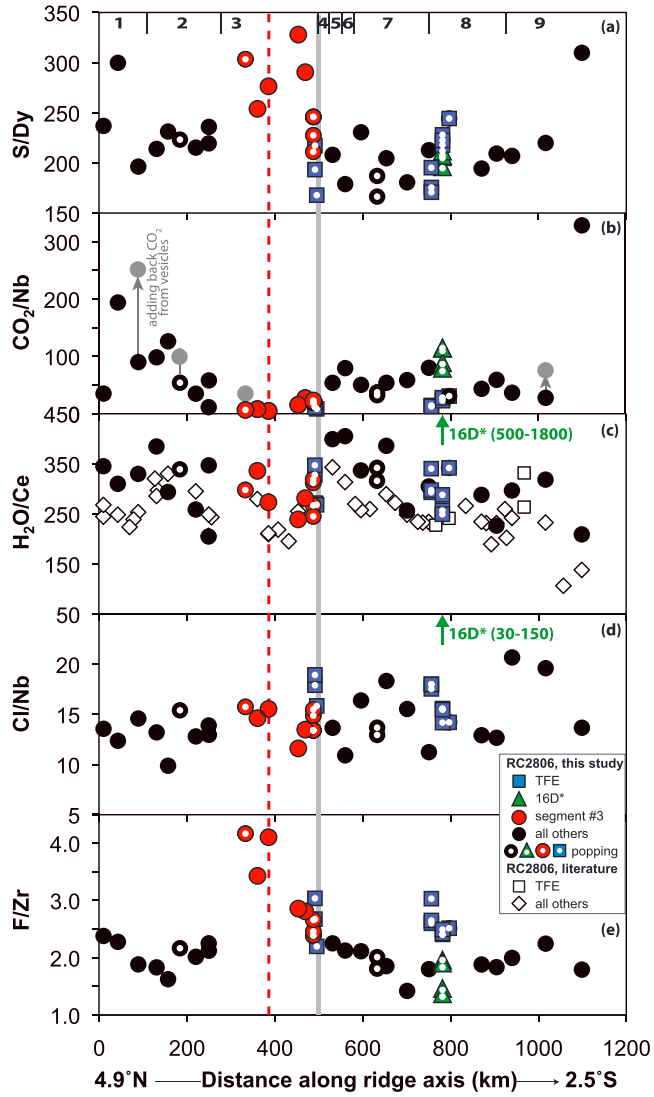

Figure 7. (a) S/Dy, (b) CO_2/Nb, (c) H_2O/Ce, (d) Cl/Nb, and (e) F/Zr as a function of distance along the ridge axis. In Figure 7b, we added back the CO_2 measured in the vesicles of four samples to calculate the total CO_2/Nb corrected from degassing (grey circles, vesicles CO_2 content from *Tucker et al.* [2012]). In Figure 6c, literature values for H_2O are from *Schilling* [2014]. The red dotted line indicates the latitude of maximum influence of the Sierra Leone Plume, and the grey line indicates the latitude of the St. Paul fracture zone.

saturation can vary as a function of melt composition (principally FeO), temperature, and pressure [*O'Neill and Mavrogenes*, 2002; *Liu et al.*, 2007]. We tested these effects using the *O'Neill and Mavrogenes* [2002] and *Liu et al.*'s [2007] models (equations (27) and (9), respectively). Although the *O'Neill and Mavrogenes* [2002] model partially accounts for the lower S for two of the 16D* samples (16D-5 g and 16D-1 g, that have lower MgO and CaO contents), the effect of melt composition from both models fails to account for the 300 ppm S gap between the four 16D* samples and the other RC2806 samples. Using the *Liu et al.* [2007] model, both a decrease of 100°C and an increase of 1 GPa could account for the S gap. However, such strong changes in temperature or pressure should have also significantly affected the major element composition of these samples, which is not observed. In the fourth scenario, we consider that the 16D* samples were formed under similar conditions as the other RC2806 samples, at sulfide saturation, then were affected by shallow assimilation processes within the last stages of magma evolution. This contaminant could have either increased the FeO content or decreased the S content of the 16D* samples just before eruption, thus driving these samples out of equilibrium with respect to the FeO-S correlation. However, it is unlikely that this contamination is also responsible for the low REE contents of the 16D* samples. In summary, none of these scenarios fully accounts for the peculiar composition of the 16D* samples. It is possible that the 16D* samples were affected by a combination of several of these scenarios. The 16D* samples show evidence for both unusual primary melt compositions, as shown by their depleted REE patterns, and contamination by secondary processes, as shown by their high Cl/Nb (30–150, compared to <20 for other RC2806 samples, and <30 for uncontaminated MORB from northern East Pacific Rise [*le Roux et al.*, 2006]; the nature of the contaminant is further discussed in section 5.3.1), and it remains unclear which process is most directly linked to the offset in S and/or FeO contents.

5.2. Case of CO_2: Effect of Degassing

CO_2 has a very different behavior compared to S or other volatiles. Because of its low solubility in basaltic melts, MORB samples contain little dissolved CO_2 [*Dixon and Stolper*, 1995; *Fine and Stolper*, 1986]. Under the hydrostatic pressures corresponding to the depth where the samples have been dredged (from 3070 to

4665 m bsl, i.e., from 337 to 444 bar), the solubility of CO_2 in basaltic melts corresponds to a dissolved CO_2 content of 140–210 ppm [*Dixon and Stolper*, 1995]. This range is in good agreement with the amount measured in the RC2806 glasses (143–264 ppm), indicating that CO_2 has reached saturation. Moreover, most of the studied glasses contain at least 1 vesicle per glass chip, illustrating the presence of a vapor phase coexisting with the melt during the eruption. Thus, most of the variation in the CO_2 content should be due to degassing processes, and the CO_2/Nb ratio cannot be directly used as a tracer of source heterogeneity (Figure 7b).

If we compare the modeled saturation pressure with the collection pressure (taken as a proxy for eruption pressure) of each sample, we see that most RC2806 samples (except for two 16D* samples) are saturated to slightly oversaturated (up to 1.6 times the CO_2 content at saturation; Figure 5b), with a CO_2-rich vapor phase containing 96% CO_2, 4% H_2O, on average [*Dixon and Stolper*, 1995]. This result confirms that part of the CO_2 has already been lost to the gas phase by the time these magmas erupted. This is in good agreement with the results from *Tucker et al*. [2012], which show, using rare gas measurements, that all RC2806 samples are variably degassed and that they all have had some bubble loss. Thus, even by taking into account the amount of CO_2 from the trapped bubbles, the total CO_2 content would still represent a degassed magma (Figure 7b). Note that the amount of H_2O that partitions into the vapor phase is small and does not significantly affect the H_2O content dissolved in the melt. The oversaturated character of most of the RC2806 samples means that the melts were last in equilibrium with a vapor phase at variable depth within the crust, then evolved out of equilibrium during ascent. The oversaturation might be due to a delay in bubble nucleation and diffusion of CO_2 in the melt, because of the competition between the slow diffusion rate of CO_2 and the rapid ascent rate of the magma [*Dixon et al*., 1988]. The amount of oversaturation can be calculated by subtracting the collection pressure from the saturation pressure [e.g., *le Roux et al*., 2006]; oversaturation varies between 14 and 198 bar (Figure 5b), which corresponds to a depth in the crust between subsurface and ~700 m. Although no clear correlation is found between the degree of oversaturation and other geochemical parameters, the strongest oversaturation (1.5–1.6 times the CO_2 content at saturation) is found in samples with $<$0.4 wt % H_2O, in good agreement with the results from *Simons et al*. [2002].

The CO_2/Nb ratios of the RC2806 samples vary from 5 to 194 (average of 58, with one outlier, sample #1D-1 g, having a value of 329; Figure 7b), illustrating the large range in degree of degassing. These values are lower than those estimated for undegassed MORBs (239 ± 46 for the Siqueiros melt inclusions [*Saal et al*., 2002], ~530 for the 2πD43 Popping Rock and other MORB samples [*Cartigny et al*., 2008, and references therein]). Although the two samples with the highest CO_2/Nb ratio also have MgO contents $>$8.5 wt %, the overall absence of correlation between the CO_2/Nb ratios and the MgO contents of RC2806 samples ($R^2 = 0.13$) does not indicate any clear link between crystallization and degassing and favors shallow degassing during late-stage magma ascent [e.g., *le Roux et al*., 2006]. No correlation is found between CO_2/Nb and eruption depth or saturation pressure, indicating that equilibrium degassing only cannot account for the range in CO_2/Nb ratios in the RC28063 samples. However, there is a negative correlation between the H_2O contents and the CO_2/Nb ratios (excluding 16D* samples), which could illustrate the combined effect of (1) faster diffusion rates and (2) smaller diffusion lengths in hydrous melts with greater vesicularity [*Simons et al*., 2002]. This is in good agreement with the fact that samples from segment #3 and TFE samples have the highest H_2O contents and the lowest CO_2/Nb ratios (true even if the CO_2 from vesicles is taken into account; Figure 7b [*Tucker et al*., 2012]). Alternatively, the low CO_2/Nb ratios in samples from segment #3 and TFE samples could also be due to a higher Nb content in the source (see section 5.4.3). Regardless of the amount of degassing that affected each sample, we observe an overall positive correlation between the CO_2 content and the eruption pressure. This result is opposite to results from *Dixon et al*. [1988] from Juan de Fuca MORB (local study containing on- and off-axis samples) but consistent with the global study of on-axis MORB from *Chavrit et al*. [2012].

5.3. Small-Scale Variations

5.3.1. Case of the 16D* Samples: Shallow Assimilation of Hydrothermal Fluids

The 16D* samples plot as outliers in Figure 6, indicating that either they are not cogenetic to the rest of the RC2806 samples, or they originate from the same source, but evolved differently later on. Because they all come from the same dredge site (16D, one dredge area represents less than 2 km along the ridge axis

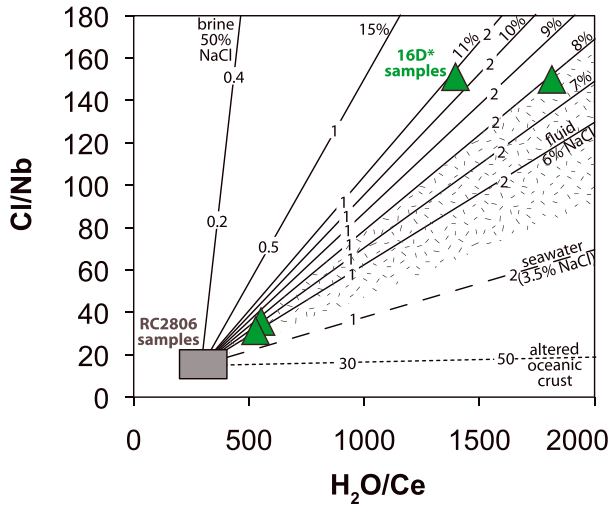

Figure 8. Cl/Nb versus H_2O/Ce for 16D* samples (triangles) as well as all other RC2806 samples (grey box). The mixing lines between the average composition of RC2806 samples and components labeled on each line are also plotted (altered oceanic crust, seawater, fluid/brines with variable salinity, and composition of each component are from *le Roux et al.* [2006]). The mixing lines are graduated in percentage of the component added. The dotted area represents the salinity range of fluids released by serpentinite in subduction zones (4–8% [*Scambelluri et al.*, 2004]).

[*Schilling et al.*, 1994]), we infer that they were affected either by very small scale heterogeneities or by very localized secondary processes.

The 16D* samples have low $Fe^{3+}/\Sigma Fe$, contrasting volatile element compositions, and strong depletion in most light and middle REE. It has been shown previously that depleted submarine basalts, with low initial H_2O and Cl contents, are very sensitive to any Cl and H_2O addition by seawater [e.g., *le Roux et al.*, 2006]. In Figures 6, 7c, and 7d, the 16D* samples clearly define a trend diverging from the main group of samples, with higher Cl/Nb and H_2O/Ce (30–150 and 530–1820, respectively) compared to the rest of the RC2806 samples (averages of 15 and 290, respectively). For comparison, Cl/Nb and H_2O/Ce of uncontaminated MORB samples are <30 and <500, respectively [*Michael*, 1995; *Dixon et al.*, 2002; *le Roux et al.*, 2006]. This indicates Cl and H_2O enrichment with respect to Nb and Ce, respectively, as expected for assimilation of seawater or altered material. The average Cl/H_2O of the 16D* samples (~0.027–0.038) is higher than the ratio of seawater (~0.020 [*Kent et al.*, 1999], indicating that the contaminant is different than pure seawater. Additionally, one of the 16D* samples (16D-1 g) has been previously analyzed for radiogenic isotopes, and its isotopic composition, including $^{87}Sr/^{86}Sr$ (0.702460; Table 1 of *Schilling et al.* [1994]), is indistinguishable from other RC2806 samples. This rules out direct assimilation of seawater, serpentinite [e.g., *Warren et al.*, 2009], or altered basalts as an origin for the contrasting composition of the 16D* samples. We used a mixing model based on the H_2O, Ce, Cl, and Nb contents of fluids with variable salinity (Figure 8; following *le Roux et al.* [2006]) to assess the nature of the contaminant. We find that three out of the four 16D* samples can be explained by mixing a fluid with 6–8 wt % $NaCl_{eq}$, while the fourth 16D* sample requires a fluid with slightly higher salinity (11%). This range in salinity is higher than pure seawater (~3.5%), and lower than brines described previously as potential MORB contaminants (15–50% [e.g., *Kent et al.*, 2002]), excluding these two components as potential contaminants. The salinity range of the 16D* samples is in good agreement with the salinity described for fluids released by hydrothermal vents along the Atlantic ridge system (e.g., 3.5–10% NaCl for fluids near fault zones [*Kelley and Gillis*, 1993]). Note that this salinity range is also similar to that from fluids released by serpentinite during subduction (4–8% [*Scambelluri et al.*, 2004]). Thus, we infer that the 16D* samples were contaminated by hydrothermal fluids with moderate salinity.

The 16D* samples were dredged along the ridge segment located just south of the eastern part of the Romanche transform fault. In this area, the ridge axis is poorly developed and curved. The basaltic crust is very thin or possibly absent, revealing large massifs of serpentinized peridotite [*Bonatti et al.*, 1996]. The serpentinization process results in the release of H_2-rich reduced fluids [e.g., *Janecky and Seyfried*, 1986]. Thus, it is possible that the 16D* samples assimilated reduced hydrothermal fluids released from serpentinization of the nearby peridotitic massifs. This is in good agreement with their lower $Fe^{3+}/\Sigma Fe$ (0.13 ± 0.01) compared to other RC2806 samples (0.16 ± 0.01), as H_2 addition would reduce Fe^{3+} to Fe^{2+}. This is also in good agreement with the low $^{87}Sr/^{86}Sr$ of hydrothermal fluids (0.7035 [*Elderfield and Schultz*, 1996]), compared to pure seawater. Moreover, hydrothermal fluids are also enriched in metals, including Fe [*Charlou et al.*, 2002]. Assimilation of Fe-rich, reduced fluids might have caused the contrasting FeO content of the 16D* samples (higher FeO for a given S; see Figure 5a and section 5.1). No clear enrichment in other metals such as Co or Zn is observed. Such assimilation could also have lowered the melt temperature and thus driven the S content at

sulfide saturation down (see section 5.1). Note that we cannot exclude the hypothesis of a very small scale mantle heterogeneity generating the contrasting and REE-depleted 16D* compositions. However, as only a fraction of the samples from dredge 16D are affected, we do not think that these samples result from deep mantle heterogeneity but rather from local and shallow assimilation of hydrothermal fluids. Finally, apart from 16D* samples, it is worth noting that all the other RC2806 samples do not seem to be significantly affected by Cl enrichment, compared to the widespread Cl excess in fast spreading Pacific MORBs [*Michael and Cornell*, 1998].

5.3.2. Case of the TFE Samples: Low Degree of Melting of a Heterogeneous Mantle

The TFE samples (i.e., affected by cold edge effects of nearby transform faults) are plotted as squares in Figures 6 and 7. Previous studies have shown that the presence of transform faults crosscutting the ridge axis can perturb the thermal regime, the melt budget, as well as the melt composition: at the intersection between young and hot crust and old and cold lithosphere, the rift valley deepens, the amount of melt produced decreases, and the produced basalts are richer in incompatible elements [e.g., *Fox and Gallo*, 1984; *Bender et al*., 1984; *Langmuir and Bender*, 1984]. In terms of volatile elements, basalts affected by the transform fault effect are often wetter [e.g., *Ligi et al*., 2005]. Our results are in good agreement with previous studies, as the TFE samples from the equatorial MAR are enriched in incompatible trace elements (average $(La/Sm)_N$ of 1.3 as well as in H_2O, F, and Cl, compared to other RC2806 samples.

What causes the volatile enrichment in the TFE samples? Although assimilation of seawater or hydrothermally altered material could have caused enrichments in H_2O and Cl, it could not account for enrichments in F as well as other incompatible trace elements such as Nb and Ce. The low-degree melting of the TFE samples (average of 7%, compared to 10% for other RC2806 samples) could be partially responsible for the volatile and trace element enrichment of the TFE samples. However, a 3% difference in melting degree would only account for TFE being 30 to 40% richer (using partition coefficients from *Kelley et al*. [2003]), which is smaller than what is observed (H_2O, F, and Cl are enriched by 50–250% in TFE). Low degree of melting would also not account for the high F/Zr and Cl/Nb of the TFE samples. These require a second mantle component, enriched in incompatible trace elements as well as in volatile elements. This is in good agreement with the high Pb and Sr isotope compositions of TFE samples, as described by *Schilling et al*. [1994], who interpreted the enriched composition of TFE samples as the result of the combined effects of low-degree melting and preferential sampling of volatile- and radiogenic isotope-enriched lumps or veins from a heterogeneous mantle. Thus, we interpret the high volatile contents of TFE samples as resulting from the combined effect of (1) low-degree melting and (2) source enrichment in incompatible trace elements as well as in volatile elements, as low degree of melting would preferentially sample enriched components.

5.4. Large-Scale Variations

5.4.1. 1.7°N Anomaly: Influence of the Sierra Leone Hot Spot

Previous studies have described gradients in major, trace elements, and crustal thickness that are related to the high degree of melting around 1.7°N compared to nearby segments [*Schilling et al*., 1995]. The higher degree of melt has been attributed to the current position of the hot spot associated with the Sierra Leone mantle plume [*Schilling et al*., 1994, 1995; *Hannigan et al*., 2001; *Kelley et al*., 2013]. Superimposed on this melting effect, gradients in trace element ratios and radiogenic isotopes indicate the presence of an enriched, HIMU-type mantle component in segment #3 (such as $^{206}Pb/^{204}Pb$ up to 20.1, $^{87}Sr/^{86}Sr$ up to 0.7030, and $^{3}He/^{4}He$ down to 6.77 [*Schilling et al*., 1994; *Kelley et al*., 2013]), also attributed to the presence of the nearby plume. We have shown that basalts around 1.7°N are also enriched in H_2O, F, and Cl relative to nearby segments (Figure 3). Volatile enrichment could not be produced by the higher extents of melting observed in this area, emphasizing the presence of volatile heterogeneity in the mantle beneath segment #3. In Figure 7, we see that there is no variation in H_2O/Ce and Cl/Nb around 1.7°N. These observations suggest that the higher volatile concentrations and similarly higher trace element concentrations found near 1.7°N are both due to source enrichment (described more in detail in section 5.4.3). *Simons et al*. [2002] described both H_2O and Ce enrichments but constant H_2O/Ce in the source MORB samples near the Salas Y Gomez seamount chain in the eastern Pacific, interpreted as the presence of a more fertile mantle source region sampled by the plume, compared to the surrounding depleted mantle. In contrast to the uniform H_2O/Ce and Cl/Nb ratios, we see a very sharp increase in F/Zr from an average of 2.0 and 2.3 in segments #2 and #4, respectively, up to 4.1 for samples in segment #3 (Figure 7). These samples also have some of the highest $(La/Sm)_N$ and $^{206}Pb/^{204}Pb$ of this area (Figure 1). We find a very good positive correlation between F/Zr and

$^{206}Pb/^{204}Pb$ ($R^2 = 0.72$) and negative correlation between F/Zr and $^{3}He/^{4}He$ ($R^2 = 0.61$) for samples from segments #1 to #4 (i.e., area of influence of the HIMU-type plume, i.e., a signature of old, recycled oceanic crust in the source of the Sierra Leone Plume). The fact that we also find high F/Zr in these samples indicates that high F/Zr could be a characteristic of HIMU-type mantle component and that this recycling process could possibly fractionate F from Zr.

5.4.2. Cold Zone and Gradient South of Romanche

Schilling et al. [1994, 1995] have interpreted the gradients in major, trace, and radiogenic isotope compositions from the St. Paul transform fault toward the south as the result of an increase in potential temperature of about 70°C combined with a heterogeneous mantle source. From segment #5 to #9, the mean degree of partial melting increases from 7% to 10% (Figure 1c). Volatile and radiogenic Pb-rich lumps or veins from a heterogeneous mantle are preferentially sampled by the lowest degrees of melting in the north and progressively diluted toward the south.

Our results indicate that H_2O and F decrease similarly to other incompatible elements along this 600 km long ridge area (Figure 3), with an average decrease rate of 400 and 18 ppm/100 km ($R^2 = 0.57$ and 0.45, respectively). This confirms that H_2O and F behave as nonvolatile, incompatible elements during mantle melting and magma evolution in this ridge area, and that they are not affected by degassing or secondary contamination. Therefore, due to the lower degree of melt production, basalts near the St. Paul transform zone are wetter and more enriched than the ones from the southernmost segment #9. Although we also expect the same to be true for Cl, there is no clear variation in Cl content along the ridge axis of segments #5 to #9: their average Cl content (65 ± 33 ppm, 1 SD) is similar to the samples from segments #1 and #2 that are unaffected by plume influence (60 ± 25 ppm, 1 SD).

Figure 7 shows that H_2O/Ce and F/Zr also progressively decrease toward the south. This indicates source heterogeneity in volatile contents: the enriched veins or lumps sampled along this gradient seem to be enriched in H_2O and F (with respect to Ce and Zr, respectively) compared to the surrounding depleted mantle (composition of the depleted mantle described in section 5.4.3). No zonation in Cl/Nb is observed (Figure 7d), which could indicate that these mantle heterogeneities are not enriched in Cl (with respect to Nb). Two samples (5D-1 g and 3D-2 g) have Cl/Nb slightly higher (~20) than the other samples from segments #5 to #9 (14 ± 2, 1 SD) and could be affected by very small amounts of assimilation of seawater-derived components. The Cl enrichment is 1 order of magnitude lower than the one affecting the 16D* samples and illustrates the fact that MORBs are very sensitive to assimilation of Cl-rich components due to their very low Cl content. If we only consider the H_2O and F source enrichments, we see that this heterogeneity has contrasting volatile and trace element compositions compared to the enrichment in segment #3 caused by the Sierra Leone plume (high F/Zr but constant H_2O/Ce). This result indicates a strong separation between the mantle domains situated north and south of the St. Paul fracture area, with contrasting trace elements and isotopic compositions as well as volatile element compositions. *Schilling et al.* [1994] suggested that the origin of the heterogeneities found south of the St. Paul fracture area might be due to the delamination of another, more distant plume, or the presence of subcontinental mantle lithosphere in this cold area.

The respective enrichments in F and H_2O found both in the melts and in the mantle source of MORBs from segments #5 to #9 are in very good agreement with morphotectonic ridge parameters (Figure 9 and Table S2 in the supporting information [*Klein and Langmuir*, 1987]). For instance, H_2O, F, H_2O/Ce, and F/Zr correlate negatively with segment length (R^2 of 0.7–0.9), positively with the ridge bathymetry (R^2 of 0.4–0.6), and positively with $Na_{(8)}$ (R^2 of 0.6–0.9; Figure 9). The correlations of ridge parameters with H_2O or F contents can be explained similarly to those with $Na_{(8)}$, i.e., by a progressive increase in the source potential temperature from segment #5 to segment #9 (70°C [*Schilling et al.*, 1995]). However, this is not the case for the correlations between ridge parameters and H_2O/Ce or F/Zr. As these are ratios of trace elements with similar incompatibility, an increase in potential temperature, thus in degree of melting, cannot explain the variations in H_2O/Ce or F/Zr observed from segments #5 to #9 (Figure 9). One alternate explanation could be variation in the trace element and radiogenic isotope composition of the mantle source in this area [*Schilling et al.*, 1994; *Hannigan et al.*, 2001]. *Schilling et al.* [1994, 1995] described the link between potential temperature and radiogenic isotopes along this area as a dilution effect of melts from volatile and radiogenic Pb-rich lumps: low-degree melts in segment #5 preferentially sample this enriched lithology, whereas higher-degree melts toward segment #9 would dilute these melts with larger

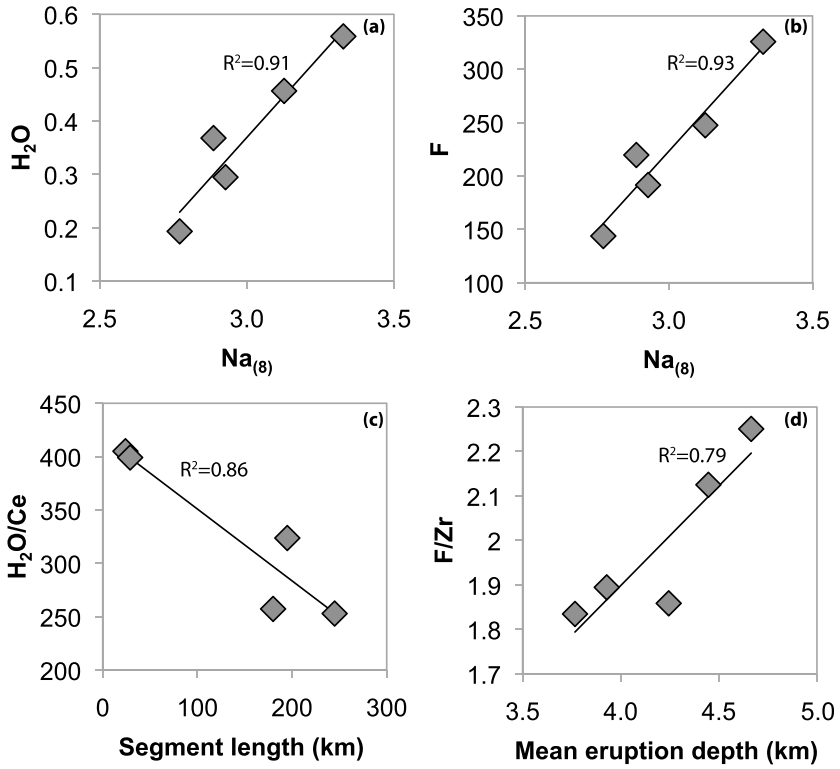

Figure 9. (a) H_2O and (b) F as a function of $Na_{(8)}$, (c) H_2O/Ce as a function of segment length, and (d) F/Zr as a function of mean eruption depth, for averages of segments #5 to #9. R^2 is the coefficient of determination for the linear regression model. $Na_{(8)}$ is calculated using Na_2O and MgO contents from *Schilling et al.* [1995], following *Bézos et al.* [2009] and *Langmuir et al.* [1992]. The segment length and mean eruption depth are from *Schilling et al.* [1995].

amounts of melts from the surrounding depleted mantle, thus creating correlated gradients between source variations, geochemistry, and ridge morphotectonic parameters. Thus, it is possible that some source variability in volatile elements is also present. This strengthens the dependency between tracers of melting processes (such as the amount of H_2O and F in basalts) and tracers of source variations (such as H_2O/Ce and F/Zr) along this part of the equatorial MAR. However, we do not observe clear, direct relationships between H_2O/Ce and F/Zr with radiogenic isotope ratios in samples from segments #5 to #9 (unlike those described above for samples from segment #3). Finally, correlations between parameters affected by variations in melting degree (such as $Na_{(8)}$, H_2O, and F) are stronger than those affected by source variations (such as H_2O/Ce or F/Zr). Therefore, we suggest that the compositional gradients result dominantly from the melting gradient and only secondarily from source variations.

5.4.3. Volatile Element Composition of the Main Mantle Components Beneath the Equatorial MAR

We described above two main mantle domains in terms of volatile element zonation along the equatorial MAR. In this section we discuss the source variations in H_2O/Ce, F/Zr, and Cl/Nb compared to known values from the literature, then use the two samples with the most enriched (40D-9 g) and the most depleted (1D-1 g) compositions to calculate the total range in volatile contents of the mantle beneath equatorial MAR. South of the Equator is a 600 km long area of depleted mantle containing veins or lumps of volatile-rich material. Basalts situated south of this domain originated from higher degrees of melting that dilute the volatile-rich material and make their composition one of the most depleted in the world. The most depleted of these samples is RC2806 1D-1 g, with H_2O/Ce of 209, F/Zr of 1.8, and Cl/Nb of 13.7. The low H_2O/Ce value of 1D-1 g is within the global MORB range (155–213 ± 40, except for north MAR, 240–280 ± 40 [*Michael*, 1995]). Most of the RC2806 samples have higher H_2O/Ce values that are representative of the high H_2O/Ce described in the northern MAR [*Michael*, 1995]. These values are higher than those for Pacific MORB (~150 [*Dixon et al.*, 2002; *Simons et al.*, 2002]). The Cl/Nb of RC2806 samples are among the lowest recorded for uncontaminated MORB (<30 [*le Roux et al.*, 2006]), and F/Zr values are slightly lower but consistent with those from the East

Pacific Rise (2.0–2.5 [*le Roux et al*., 2006]). We used the volatile contents of 1D-1 g to model the volatile composition of the modern depleted asthenosphere unpolluted by plumes. First, as the MgO content of sample 1D-1 g is ~8 wt %, we assumed that only olivine is fractionated from this melt, and we used PriMelt2 [*Herzberg and Asimow*, 2008] to calculate the amount of olivine fractionation (16.5%) in order to reach primary melt composition at equilibrium with depleted MORB mantle (DMM) [*Workman and Hart*, 2005]. Then, we back calculated the F, H_2O, and Cl contents of the primary melt (68, 689, and 6 ppm, respectively), assuming that these volatiles were completely incompatible in olivine. Finally, we used mantle/melt bulk partition coefficients similar to those for Zr, Ce, and Nb, respectively, (0.03, 0.011, and 0.003 [*Kelley et al*., 2003]) and the degree of melting estimated from $Na_{(8)}$ (15% for 1D-1 g) to calculate the composition of the mantle source. We obtained the concentrations of 12 ppm F, 110 ppm H_2O, and 1 ppm Cl. Our H_2O and F values are very consistent with the previous estimates for DMM (110 ± 50 ppm H_2O [*Workman and Hart*, 2005] and 116 ± 58 ppm H_2O and 11 ± 5 ppm F [*Salters and Stracke*, 2004]), and our Cl estimate is slightly higher (0.38 ± 0.25 [*Workman and Hart*, 2005] and 0.5 ± 0.1 ppm Cl [*Salters and Stracke*, 2004]). For comparison, *Saal et al*. [2002] obtained depleted mantle compositions for the source of the Siqueiros melt inclusions that are consistent with the depleted source from this study with respect to its H_2O and Cl contents (142 ± 85 ppm H_2O and 1 ± 0.5 ppm Cl) but slightly lower with respect to its F content (16 ± 3 ppm F). Other MORB studies estimated that DMM contained ~100 ppm H_2O on average [*Dixon et al*., 2002], with variations at the local scale (54–120 ppm H_2O and 1.7–4.5 ppm Cl for DMM beneath the Easter Microplate, southeastern Pacific [*Simons et al*., 2002]). *Le Roux et al*. [2006] obtained DMM compositions beneath the East Pacific Rise (8–14°N; 128 ± 5 ppm H_2O, 5 ± 1 ppm Cl, and 17 ± 1 ppm F) that are higher than those from this study.

The second mantle domain described in this study corresponds to a large thermal and chemical heterogeneity centered on 1.7°N that is linked to the current position of the Sierra Leone plume. Sample 40D-9 g (H_2O/Ce of 273, F/Zr of 4.1, and Cl/Nb of 15.6) is the basalt with both the strongest enrichment in $^{206}Pb/^{204}Pb$ and F/Zr. Previous studies have shown that plume-influenced MORB can have higher H_2O/Ce than DMM [*Dixon et al*., 2002], which is not observed here: the H_2O/Ce (and Cl/Nb) of sample 40D-9 g are within errors of those from the most depleted sample 1D-1 g and are consistent with previously published values for DMM as described above. On the contrary, the high F/Zr sample 40D-1 g has not been described elsewhere (F/Zr $<$ 3 in East Pacific Rise for comparison [*Le Roux et al*., 2006]), and this could be a useful tracer of enriched material in the source of MORB. We used the volatile contents of 40D-9 g (8.6% MgO) to calculate the maximum volatile enrichment of the mantle source, following the same procedure as described above. We corrected the composition for 14.0% olivine fractionation to obtain the F, H_2O, and Cl content of the primary melt (446, 7697, and 402 ppm, respectively). Then we used the estimated melting degree (9%) to calculate the composition of the enriched mantle component (52 ppm F, 770 ppm H_2O, and 37 ppm Cl). Relative to the depleted mantle end-member modeled above, the enriched mantle end-member contains ~4 times more F, 7 times more H_2O, and ~40 times more Cl. For comparison, previous studies estimated H_2O and Cl contents of ~750 ppm and 40 ppm, respectively, for the mantle beneath ridges influenced by the Salas y Gomez plume [*Simons et al*., 2002], 700–750 ppm H_2O near the Azores plume [*Dixon et al*., 2002; *Asimow et al*., 2004], 620–920 ppm H_2O beneath Iceland [*Nichols et al*., 2002], and 110–240 ppm H_2O near the Galapagos hot spot [*Cushman et al*., 2004]. Although this mantle end-member is enriched in H_2O and Cl, it is also enriched in Ce and Nb (2.8 and 2.4 ppm, respectively, compared to 0.5 and 0.1 for the depleted mantle end-member), with an enrichment factor similar to that of H_2O and Cl, consistent with the lack of H_2O/Ce and Cl/Nb gradients in this area. On the contrary, the Zr enrichment (13 ppm, compared to 7 ppm for the depleted mantle end-member) is much smaller than the one in F. Thus, the increase in F/Zr is mostly due to the higher F content in the mantle beneath segment #3. Note that the estimated Nb, Ce, and Zr of the enriched mantle end-member are 2, 4, and 10 times higher than the E-DMM estimates from *Workman and Hart* [2005], respectively.

5.5. Comparison Between the Compositions of the RC2806 Popping and Nonpopping Samples

This study allows the comparison of the chemical compositions between the 20 RC2806 "popping samples" (samples with white dots, Figures 1–7) with the rest of the RC2806 samples. Our results show that the trace and volatile element compositions, as well as the average $Fe^{3+}/\Sigma Fe$ ratios, of the RC2806 popping samples

are identical to those from other RC2806 samples. No difference has been found either for the major element and the isotopic compositions [*Schilling et al*., 1994, 1995] or for the rare gas content in their vesicles [*Tucker et al*., 2012]. Thus, they seem to resemble normal MORB samples, despite their exploding behavior (J. G. Schilling, personal communications).

The 20 popping samples from this study represent an important data set because of the scarce occurrence of this type of sample worldwide. Popping rock 2πD43 is widely used as a reference for the canonical definition of volatile contents in MORBs and in the depleted mantle [e.g., *Staudacher et al*., 1989; *Moreira et al*., 1998; *Cartigny et al*., 2008]. Thus, it is important to compare our results with 2πD43. Note that popping rock 2πD43 is one of the most enriched MORB globally in trace elements ($(La/Sm)_N$ of 1.9), and this enrichment is also reflected in its dissolved volatile element composition (177 ppm CO_2, 0.66 wt % H_2O, 567 ppm F, 948 ppm S, and 311 ppm Cl; Table S1 in the supporting information). The total volatile contents resulting from previous studies of 2πD43 are a combination of volatiles dissolved in the glass and present as gas in vesicles (17–18 vol % vesicles, containing 14300 ppm CO_2, negligible H_2O [*Cartigny et al*., 2008]; S, F, and Cl have not been measured in the 2πD43 vesicles to our knowledge). Thus, the majority of the CO_2 is found in vesicles, with only a small amount (1% of the total CO_2) found dissolved in the glass. The CO_2 contents dissolved in the glass of the RC2806 popping samples (average of 205 ppm CO_2) are similar to the one from 2πD43. However, the CO_2 present in the vesicles of the RC2806 samples (317 ppm CO_2, average of two RC2806 popping samples [*Tucker et al*., 2012]) is 2 orders of magnitude lower than in the vesicles of 2πD43. This is mostly due to the difference in vesicularity for both samples: unlike 2πD43, the RC2806 popping samples contain 0–2 vol % vesicles, typical of MORB glasses (0–5 vol % for Atlantic MORBs [*Chavrit et al*., 2012]). *Tucker et al*. [2012] have shown that all RC2806 samples are partially degassed and have lost part of their initial vesicle content (vesicle migration). Thus, it remains uncertain why both the 2πD43 and RC2806 popping samples exploded on the deck of the ship, as their vesicularity and volatile compositions are so distinct. Their explosive behavior might not solely result from a high amount of gas or vesicles but may result from other parameters (e.g., speed of dredge basket ascent from the seafloor or amount of cracks and permeable pathways in the rock).

If the high volatile content of the 2πD43 popping rock is not the origin of its exploding behavior, then several questions arise: (1) what causes the high vesicularity of 2πD43? and (2) are the volatiles from 2πD43 representative of an undegassed MORB magma? One simple explanation is that the high vesicularity of 2πD43 is a result of bubble migration and accumulation in this particular sample. Although this cumulative origin has been denied on the basis of vesicle size distribution analysis [*Sarda and Graham*, 1990], it has also been questioned [*Javoy and Pineau*, 1991] and supported by other studies based on helium isotopes [e.g., *Moreira and Kunz*, 2013] and MORB vesicularity parameterization at the global scale [*Chavrit et al*., 2014]. Our study underlines once again that 2πD43 is unique compared not only to all MORB glasses but also to other popping samples such as RC2806. Thus, our study favors the origin of 2πD43 volatiles in an overabundance of vesicles. Even though 2πD43 is a unique sample for the study of noble gas ratios in the mantle, the possibility of bubble accumulation questions its use a reference for the CO_2 content of undegassed MORB.

6. Conclusions

By using high precision, in situ volatile and trace element measurements, together with previously published major, trace, and isotopic data, we interpret the variations in volatile elements along the equatorial MAR as a combination of multiple primary and secondary processes.

1. The RC2806 samples are saturated in sulfide phases. Under reduced MORB conditions, most, if not all, S is present as S^{2-}, and the S content at sulfide saturation is mostly controlled by the amount of FeO in the melt, which causes the very good correlations between FeO and S contents, similar to other MORB samples.
2. The CO_2 in all samples is strongly affected by degassing and CO_2/Nb variations most likely track variable extents of kinetic degassing. Saturation with a CO_2 volatile phase was reached up to 700 m depth within the crust. At the depth of eruption on the seafloor, the RC2806 samples are saturated to oversaturated with respect to CO_2, possibly due to delay of bubble formation and/or growth.
3. Four samples from one single dredge (16D) have contrasting volatile element compositions. They are enriched in Cl and H_2O, with respect to Nb and Ce, but they are very depleted in most other incompatible

elements, including F. They also have significantly reduced $Fe^{3+}/\Sigma Fe$ ratios, 3 sigma below the global average for MORB glasses. We interpret this to be the result of contamination by reduced hydrothermal fluids, most likely produced by serpentinization of nearby peridotite massifs.

4. A subset of samples dredged near fracture zones shows strong enrichment in volatile element compositions, as well as high F/Zr (and Cl/Nb). The enrichment in volatiles is the consequence of the effect of very low degree melts of a mantle source containing small-scale heterogeneities enriched in F and maybe Cl (with respect to Zr and Nb, respectively).
5. The strongest variation in volatile element compositions is found in samples from segment #3. The symmetrical enrichment around the latitude of maximum influence of the Sierra Leone hot spot track (1.7°N) is linked to source heterogeneity. The mantle in this area is enriched in trace elements as well as in H_2O, F, and Cl. The strong increase in F/Zr indicates a fractionation of F compared to Zr, which correlates with the $^{206}Pb/^{204}Pb$ anomaly around this HIMU-type plume. We interpret this high F/Zr, with no associated increase in H_2O/Ce, as the result of ancient recycled crust that has undergone strong dehydration during subduction.
6. The large cold zone present south of the Equator is heterogeneous in terms of its H_2O and F contents, resulting in gradual increase of H_2O, F, H_2O/Ce, and F/Zr with decreasing degree of melting toward the St. Paul fracture zone. The nature of mantle source compositional heterogeneity in this area is different from the one north of the St. Paul fracture zone. These variations in volatile contents and ratios are well correlated with morphotectonic ridge parameters and are caused by the combined effect of (1) the variation in degree of melting and (2) the progressive dilution effect that arises during the melting of a heterogeneous source containing veins or lumps of material enriched in H_2O and F (with respect to Ce and Zr, respectively) within a depleted mantle.
7. The 20 RC2806 popping samples are identical in terms of volatile contents dissolved in the glass to other RC2806 samples. They also have dissolved volatile contents comparable to the ones from the 2πD43 popping rock. Their vesicularity is low (a few percent) and similar to those of the RC2806 nonpopping samples as well as all MORB samples, with the exception of the 2πD43 popping rock (17–18%). The comparison between the RC2806 popping samples and the 2πD43 popping rock shows that there is no direct link between measured vesicularity and exploding behavior. We therefore question the use of 2πD43 as a reference for undegassed CO_2 MORB magma volatile composition.

Acknowledgments

Data supporting this study is available in the supporting information. The authors would like to thank T. Gooding for the advice during the sample preparation, J. Wang for the precious help with the SIMS, M. Lytle for the support with the LA-ICP-MS, as well as J. Tucker, D. Chavrit, and S. Lambart for the constructive discussions. J. Dixon and P. le Roux are thanked for their thoughtful reviews and M. Walter for the editorial handling. This work was funded by the Deep Carbon Observatory, Reservoirs and Fluxes Directorate. The use of the NSLS was supported by DOE under contracts DE-AC02-98CH10886 and DE-FG02-92ER14244.

References

Asimow, P. D., J. E. Dixon, and C. H. Langmuir (2004), A hydrous melting and fractionation model for mid-ocean ridge basalts: Application to the Mid-Atlantic Ridge near the Azores, *Geochem. Geophys. Geosyst.*, *5*, Q01E16, doi:10.1029/2003GC000568.

Bender, J. F., C. H. Langmuir, and G. N. Hanson (1984), Petrogenesis of basalt glasses from the Tamayo region, East Pacific Rise, *J. Petrol.*, *25*, 213–254, doi:10.1093/petrology/25.1.213.

Bézos, A., S. Escrig, C. H. Langmuir, P. Michael, and C. H. Langmuir (2009), Origins of chemical diversity of back-arc basin basalts: A segment-scale study of the Eastern Lau Spreading Center, *J. Geophys. Res.*, *114*, B06212, doi:10.1029/2008JB005924.

Bonatti, E., A. Peyve, P. Kepezhinskas, N. Kurentsova, M. Seyler, S. Skolotnev, and G. Udintsev (1992), Upper mantle heterogeneity below the Mid-Atlantic Ridge, 0–15°N, *J. Geophys. Res.*, *97*, 4461–4476, doi:10.1029/91JB02838.

Bonatti, E., M. Ligi, G. Carrara, L. Gasperini, N. Turko, S. Perfiliev, A. Peyve, and P. F. Sciuto (1996), Diffuse impact of the Mid-Atlantic Ridge with the Romanche transform: An ultracold ridge-transform intersection, *J. Geophys. Res.*, *101*(B4), 8043–8054, doi:10.1029/95JB02249.

Cartigny, P., F. Pineau, C. Aubaud, and M. Javoy (2008), Towards a consistent mantle carbon flux estimate: Insights from volatile systematics (H_2O/Ce, δD, CO_2/Nb) in the North Atlantic mantle (14°N and 34°N), *Earth Planet. Sci. Lett.*, *265*, 672–685, doi:10.1016/j.epsl.2007.11.011.

Charlou, J. L., J. P. Donval, Y. Fouquet, P. Jean-Baptiste, and N. Holm (2002), Geochemistry of high H2 and CH4 vent fluids issuing from ultramafic rocks at the Rainbow hydrothermal field (36°14′N, MAR), *Chem. Geol.*, *191*, 345–359, doi:10.1016/S0009-2541(02)00134-1.

Chavrit, D., E. Humler, Y. Morizet, and D. Laporte (2012), Influence of magma ascent rate on carbon dioxide degassing at oceanic ridges: Message in a bubble, *Earth Planet. Sci. Lett.*, *357–358*, 376–385, doi:10.1016/j.epsl.2012.09.042.

Chavrit, D., E. Humler, and D. Grasset (2014), Mapping modern CO_2 fluxes and mantle carbon content all along the mid-ocean ridge system, *Earth Planet. Sci. Lett.*, *387*, 229–239, doi:10.1016/j.epsl.2013.11.036.

Cottrell, E., and K. A. Kelley (2011), The oxidation state of Fe in MORB glasses and the oxygen fugacity of the upper mantle, *Earth Planet. Sci. Lett.*, *305*, 270, doi:10.1016/j.epsl.2011.03.014.

Cottrell, E., K. A. Kelley, A. Lanzirotti, and R. A. Fischer (2009), High-precision determination of iron oxidation state in silicate glasses using XANES, *Chem. Geol.*, *268*, 167, doi:10.1016/j.chemgeo.2009.08.008.

Cushman, B., J. Sinton, G. Ito, and J. E. Dixon (2004), Glass compositions, plume-ridge interaction, and hydrous melting along the Galàpagos Spreading Center, 90.5°W to 98°W, *Geochem. Geophys. Geosyst.*, *5*, Q08E17, doi:10.1029/2004GC000709.

Czamanske, G. K., and J. G. Moore (1977), Composition and phase chemistry of sulfide globules in basalts from the Mid-Atlantic Ridge rift valley near 37°N lat, *Geol. Soc. Am. Bull.*, *88*, 587–599.

Dixon, J. E., and E. M. Stolper (1995), An experimental study of water and carbon dioxide solubilities in mid-ocean ridge basaltic liquids. Part II: Application to degassing, *J. Petrol.*, *36*, 1633–1646.

Dixon, J. E., E. Stolper, and J. R. Delaney (1988), Infrared spectroscopic measurements of CO_2 and H_2O in Juan de Fuca Ridge basaltic glasses, *Earth Planet. Sci. Lett.*, *90*, 87–104.
Dixon, J. E., L. Leist, C. H. Langmuir, and J. G. Schilling (2002), Recycled dehydrated lithosphere observed in plume-influenced mid-ocean ridge basalt, *Nature*, *420*, 385–389, doi:10.1038/nature01215.
Elderfield, H., and A. Schultz (1996), Mid-ocean ridge hydrothermal fluxes and the chemical composition of the ocean, *Annu. Rev. Earth Planet. Sci.*, *24*, 191–224.
Fine, G., and E. Stolper (1986), Dissolved carbon dioxide in basaltic glasses: Concentrations and speciation, *Earth Planet. Sci. Lett.*, *76*, 263–278.
Fox, P. J., and D. G. Gallo (1984), A tectonic model for ridge-transform-ridge plate boundaries: Implications for the structure of oceanic lithosphere, *Tectonophysics*, *104*, 205–242, doi:10.1016/0040-1951(84)90124-0.
Hannigan, R. E., A. R. Basu, and F. Teichmann (2001), Mantle reservoir geochemistry from statistical analysis of ICP-MS trace element data of equatorial mid-Atlantic MORB glasses, *Chem. Geol.*, *175*, 397–428, doi:10.1016/S0009-2541(00)00335-1.
Hauri, E. H., J. Wang, J. E. Dixon, P. L. King, C. Mandeville, and S. Newman (2002), SIMS analysis of volatiles in silicate glasses 1. Calibration, matrix effects and comparisons with FTIR, *Chem. Geol.*, *18*, 99–114, doi:10.1016/S0009-2541(01)00375-8.
Hekinian, R., M. Chaigneau, and J. L. Cheminée (1973), Popping rocks and lava tubes from the Mid-Atlantic Rift Valley at 36°N, *Nature*, *245*, 371–373.
Herzberg, C., and P. D. Asimow (2008), Petrology of some oceanic island basalts: PRIMELT2.XLS software for primary magma calculation, *Geochem. Geophys. Geosyst.*, *9*, Q09001, doi:10.1029/2008GC002057.
Janecky, D. R., and W. E. Seyfried Jr. (1986), Hydrothermal serpentinization of peridotite within the oceanic crust: Experimental investigations of mineralogy and major element chemistry, *Geochim. Cosmochim. Acta*, *50*, 1357–1378, doi:10.1016/0016-7037(86)90311-X.
Javoy, M., and F. Pineau (1991), The volatiles record of a "popping" rock from the Mid-Atlantic Ridge at 14°N: Chemical and isotopic composition of gas trapped in the vesicles, *Earth Planet. Sci. Lett.*, *107*, 598–611, doi:10.1016/0012-821X(91)90104-P.
Jenner, F. E., H. C. O'Neill, J. R. Arculus, and J. A. Mavrogenes (2010), The magnetite crisis in the evolution of arc-related magmas and the initial concentration of Au, Ag and Cu, *J. Petrol.*, *51*(12), 2455–2466, doi:10.1093/petrology/egq063.
Jenner, F. E., R. J. Arculus, J. A. Mavrogenes, N. J. Dyriw, O. Nebel, and E. H. Hauri (2012), Chalcophile element systematics in volcanic glasses from the northwestern Lau Basin, *Geochem. Geophys. Geosyst.*, *13*, Q06014, doi:10.1029/2012GC004088.
Jugo, P. J., W. Wilke, and R. Botcharnikov (2010), Sulfur K-edge XANES analysis of natural and synthetic basaltic glasses: Implications for S speciation and S content as function of oxygen fugacity, *Geochim. Cosmochim. Acta*, *74*, 5926–5938, doi:10.1016/j.gca.2010.07.022.
Kelley, D. S., and K. M. Gillis (1993), Fluid evolution in submarine magma-hydrothermal systems at the Mid-Atlantic Ridge, *J. Geophys. Res.*, *98*, 19,579–19,596, doi:10.1029/93JB01432.
Kelley, K. A., T. Plank, J. Ludden, and H. Staudigel (2003), Composition of altered oceanic crust at ODP Sites 801 and 1149, *Geochem. Geophys. Geosyst.*, *4*(6), 8910, doi:10.1029/2002GC000435.
Kelley, K. A., R. H. Kingsley, and J.-G. Schilling (2013), Composition of plume-influenced mid-ocean ridge lavas and glasses from the Mid-Atlantic Ridge, East Pacific Rise, Galápagos Spreading Center, and Gulf of Aden, *Geochem. Geophys. Geosyst.*, *14*, 223–242, doi:10.1002/ggge.20049.
Kent, A. J. R., M. D. Norman, I. D. Hutcheon, and E. M. Stolper (1999), Assimilation of seawater-derived components in an oceanic volcano: Evidence from matrix glasses and glass inclusions from Loihi seamount, Hawaii, *Chem. Geol.*, *156*, 299–319, doi:10.1016/S0009-2541(98)00188-0.
Kent, A. J. R., D. W. Peate, S. Newman, E. M. Stolper, and J. A. Pearce (2002), Chlorine in submarine glasses from the Lau Basin: Seawater contamination and constraints on the composition of slab-derived fuids, *Earth Planet. Sci. Lett.*, *202*, 361–377.
Klein, E. M., and C. H. Langmuir (1987), Global correlations of ocean ridge basalt chemistry with axial depth and crustal thickness, *J. Geophys. Res.*, *92*, 8089–8115, doi:10.1029/JB092iB08p08089.
Kress, V. C., and I. S. E. Carmichael (1991), The compressibility of silicate liquids containing Fe_2O_3 and the effect of composition, temperature, oxygen fugacity and pressure on their redox states, *Contrib. Mineral. Petrol.*, *108*, 82–92, doi:10.1007/BF00307328.
Langmuir, C. H., and J. F. Bender (1984), The geochemistry of oceanic basalts in the vicinity of transform faults: Observations and implications, *Earth Planet. Sci. Lett.*, *69*, 107–127, doi:10.1016/0012-821X(84)90077-3.
Langmuir, C. H., E. M. Klein, and T. Plank (1992), Petrological systematics of mid-ocean ridge basalts: Constraints on melt generation beneath ocean ridges, *Geophys. Monogr.*, *91*, 193–280.
le Roux, P. J., S. B. Shirey, E. H. Hauri, M. R. Perfit, and J. R. Bender (2006), The effects of variable sources, processes, and contaminants on the composition of northern EPR MORB (8–10°N and 12–14°N): Evidence from volatiles (H_2O, CO_2, S) and halogens (F, Cl), *Earth Planet. Sci. Lett.*, *251*, 209–231, doi:10.1016/j.epsl.2006.09.012.
Li, C., and A. J. Naldrett (1993), Sulfide capacity of magma: A quantitative model and its application to the formation of sulfide ores at Sudbury, *Ondario. Econ. Geol.*, *88*, 1253–1260, doi:10.2113/gsecongeo.88.5.1253.
Ligi, M., E. Bonatti, A. Cipriani, and L. Ottolini (2005), Water-rich basalts at mid-ocean ridge cold spots, *Nature*, *434*, 66–69, doi:10.1038/nature03264.
Liu, Y., N.-T. Samaha, and D. R. Baker (2007), Sulfur concentration at sulfide saturation (SCSS) in magmatic silicate melts, *Geochim. Cosmochim. Acta*, *71*, 1783–1799, doi:10.1016/j.gca.2007.01.004.
Lytle, M. L., K. A. Kelley, E. H. Hauri, J. G. Gill, D. Papia, and R. J. Arculus (2012), Tracing mantle sources and Samoan influence in the northwestern Lau back-arc basin, *Geochem. Geophys. Geosyst.*, *13*, Q10019,, doi:10.1029/2012GC004233.
Mathez, E. A. (1976), Sulfur solubility and magmatic sulphides in submarine basalt glass, *J. Geophys. Res.*, *81*(23), 4269–4276, doi:10.1029/JB081i023p04269.
McDonough, W. F., and S.-S. Sun (1995), The composition of the Earth, *Chem. Geol.*, *120*, 223–253, doi:10.1016/0009-2541(94)00140-4.
Michael, P. (1995), Regionally distinctive sources of depleted MORB: Evidence from trace elements and H_2O, *Earth Planet. Sci. Lett.*, *131*, 301–320.
Michael, P. J., and W. C. Cornell (1998), Influence of spreading rate and magma supply on crystallization and assimilation beneath mid-ocean ridges: Evidence from chlorine and major element chemistry of mid-ocean ridge basalts, *J. Geophys. Res.*, *103*, 18,325–18,356, doi:10.1029/98JB00791.
Moreira, M., and M. D. Kunz (2013), Noble gases as tracers of mantle processes and magmatic degassing, in *The Noble Gases as Geochemical Tracers*, edited by P. Burnard, pp. 371–391, Springer, Berlin.
Moreira, M., J. Kunz, and C. Allègre (1998), Rare gas systematics in popping rock: Isotopic and elemental compositions in the upper mantle, *Science*, *279*, 1178–1181, doi:10.1126/science.279.5354.1178.
Nichols, A. R. L., M. R. Carroll, and Á. Höskuldsson (2002), Is the Iceland hot spot also wet? Evidence from the water contents of undegassed submarine and subglacial pillow basalts, *Earth Planet. Sci. Lett.*, *202*, 77–87.
O'Neill, H. C., and J. A. Mavrogenes (2002), The sulfide capacity and the sulfur content at sulfide saturation of silicate melts at 1400°C and 1 bar, *J. Petrol.*, *43*(6), 1049–1087, doi:10.1093/petrology/43.6.1049.

Perfit, M. R., W. I. Ridley, and I. Jonasson (1999), Geologic, petrologic and geochemical relationships between magmatism and massive sulfide mineralization along the eastern Galapagos Spreading Center, *Rev. Econ. Geol.*, *8*, 75–100.

Pineau, F., and M. Javoy (1994), Strong degassing at ridge crests: The behavior of dissolved carbon and water in basalt glasses at 14°N Mid-Atlantic Ridge, *Earth Planet. Sci. Lett.*, *123*, 179–198, doi:10.1016/0012-821X(94)90266-6.

Pineau, F., M. Javoy, and Y. Bottinga (1976), $^{13}C/^{12}C$ ratios of rocks and inclusions in popping rocks of the Mid-Atlantic Ridge and their bearing on the problem of isotopic composition of deep seated carbon, *Earth Planet. Sci. Lett.*, *29*, 413–421, doi:10.1016/0012-821X(76)90146-1.

Ryan, W. B. F., et al. (2009), Global Multi-Resolution Topography synthesis, *Geochem. Geophys. Geosyst.*, *10*, Q03014, doi:10.1029/2008GC002332.

Saal, A. E., E. H. Hauri, C. H. Langmuir, and M. R. Perfit (2002), Vapor undersaturation in primitive mid-ocean ridge basalts and the volatile content of Earth's upper mantle, *Nature*, *419*, 451–455, doi:10.1038/nature01073.

Salters, V. J. M., and A. Stracke (2004), Composition of the depleted mantle, *Geochem. Geophys. Geosyst.*, *5*, Q05B07, doi:10.1029/2003GC000597.

Sarda, P., and D. Graham (1990), Mid-ocean ridge popping rocks: Implications for degassing at ridge crests, *Earth Planet. Sci. Lett.*, *97*, 268–289, doi:10.1016/0012-821X(90)90047-2.

Scambelluri, M., O. Müntener, L. Ottolini, T. Pettke, and R. Vannucci (2004), The fate of B, Cl and Li in the subducted oceanic mantle and in the antigorite breakdown fluids, *Earth Planet. Sci. Lett.*, *222*, 217–234.

Schilling, J. G. (1973), Iceland mantle plume: Geochemical study of Reykjanes Ridge, *Nature*, *242*(5400), 565–571, doi:10.1038/242565a0.

Schilling, J. G., M. B. Bergeron, R. Evans, and J. V. Smith (1980), Halogens in the mantle beneath the north atlantic [and discussion], *Philos. Trans. R. Soc. London, Ser. A*, *297*(1431), 147–178, doi:10.1098/rsta.1980.0208.

Schilling, J. G., M. Zajac, R. Evans, T. Johnston, W. White, J. D. Devine, and R. Kingsley (1983), Petrologic and geochemical variations along the Mid-Atlantic Ridge from 29°N to 73°N, *Am. J. Sci.*, *283*(6), 510–586, doi:10.2475/ajs.283.6.510.

Schilling, J. G., B. B. Hanan, B. McCully, R. H. Kingsley, and D. Fontignie (1994), Influence of the Sierra Leone mantle plume on the equatorial Mid-Atlantic Ridge: A Nd-Sr-Pb isotopic study, *J. Geophys. Res.*, *99*(B6), 12,005–12,028, doi:10.1029/94JB00337.

Schilling, J. G., C. Ruppel, A. N. Davis, B. McCuliy, S. A. Tighe, R. H. Kingsley, and J. Lin (1995), Thermal structure of the mantle beneath the equatorial Mid-Atlantic Ridge: Inferences from the spatial variation of dredged basalt glass compositions, *J. Geophys. Res.*, *100*(B6), 10,057–10,076, doi:10.1029/95JB00668.

Schilling, J.-G. (2014), Dissolved H_2O and Cl concentrations of basalts from the equatorial Mid-Atlantic Ridge, *Integr. Earth Data Appl.*, doi:10.1594/IEDA/100479.

Simons, K., J. E. Dixon, J.-G. Schilling, R. H. Kingsley, and R. Poreda (2002), Volatiles in basaltic glasses from the Easter-Salas y Gomez Seamount Chain and Easter Microplate: Implications for geochemical cycling of volatile elements, *Geochem. Geophys. Geosyst.*, *3*(7), doi:10.1029/2001GC000173.

Staudacher, T., P. Sarda, S. H. Richardson, C. J. Allègre, I. Sagna, and L. V. Dmitriev (1989), Noble gases in basalt glasses from a Mid-Atlantic Ridge topographic high at 14°N: Geodynamic consequences, *Earth Planet. Sci. Lett.*, *96*, 119–133, doi:10.1016/0012-821X(89)90127-1.

Taylor, B., and F. Martinez (2003), Back-arc basin basalt systematics, *Earth Planet. Sci. Lett.*, *210*, 481–497, doi:10.1016/S0012-821X(03)00167-5.

Tucker, J. M., S. Mukhopadhyay, and J.-G. Schilling (2012), The heavy noble gas composition of the depleted MORB mantle (DMM) and its implications for the preservation of heterogeneities in the mantle, *Earth Planet. Sci. Lett.*, *355–356*, 244–254, doi:10.1016/j.epsl.2012.08.025.

Wallace, P., and I. S. E. Carmichael (1992), Sulfur in basaltic magmas, *Geochim. Cosmochim. Acta*, *56*, 1863–1874.

Warren, J. M., N. Shimizu, C. Sakaguchi, H. J. B. Dick, and E. Nakamura (2009), An assessment of upper mantle heterogeneity based on abyssal peridotite isotopic compositions, *J. Geophys. Res.*, *114*, B12203, doi:10.1029/2008JB006186.

White, W. M., and J.-G. Schilling (1978), The nature and origin of geochemical variation in Mid-Atlantic Ridge basalts from the central North Atlantic, *Geochim. Cosmochim. Acta*, *42*(10), 1501–1516, doi:10.1016/0016-7037(78)90021-2.

Workman, R. K., and S. R. Hart (2005), Major and trace element composition of the depleted MORB mantle (DMM), *Earth Planet. Sci. Lett.*, *231*, 53–72, doi:10.1016/j.epsl.2004.12.005.